Paleoceanography and Paleoclimatology

RESEARCH ARTICLE
10.1029/2019PA003785

Great Basin Paleoclimate and Aridity Linked to Arctic Warming and Tropical Pacific Sea Surface Temperatures

Matthew S. Lachniet[1], Yemane Asmerom[2], Victor Polyak[2], and Rhawn Denniston[3]

[1]Department of Geoscience, University of Nevada, Las Vegas, NV, USA, [2]Department of Earth and Planetary Science, University of New Mexico, Albuquerque, NM, USA, [3]Department of Geology, Cornell College, Mount Vernon, IA, USA

Key Point:
- We show from a high-resolution speleothem record from Nevada and a regional Aridity Index that early to Middle Holocene aridity was associated with reduced arctic sea ice extent and a warm tropical Pacific Ocean driven by northern hemisphere summer insolation

Correspondence to:
M. S. Lachniet,
matthew.lachniet@unlv.edu

Citation:
Lachniet, M. S., Asmerom, Y., Polyak, V., & Denniston, R. (2020). Great Basin paleoclimate and aridity linked to Arctic warming and tropical Pacific Sea surface temperatures. *Paleoceanography and Paleoclimatology*, *35*, e2019PA003785. https://doi.org/10.1029/2019PA003785

Received 7 OCT 2019
Accepted 11 MAY 2020
Accepted article online 12 JUN 2020

Abstract The arid southwestern United States is susceptible to sustained droughts that impact water resources and economic activity for millions of residents. Previous work has not systematically investigated the structure, timing, and possible forcings of Holocene Great Basin sub-orbital hydroclimate changes, impeding our ability to understand the potential future controls on Southwestern aridity. The objective of this paper is to constrain the potential forcings on Holocene aridity and temperature, via comparison of new high-resolution speleothem data, an Aridity Index synthesizing hydroclimate records, and linkages of Southwestern paleoclimate to other regions. The high-resolution data from Leviathan Cave provide a paleoclimate record since 13,400 yr ago: A cool Younger Dryas was followed by two pronounced Middle Holocene aridity intervals between 9,850 and 5,310 yr B2k characterized by low growth rates and high $\delta^{18}O$ and $\delta^{13}C$ values. Subsequently, stalagmite $\delta^{18}O$ values show near-modern levels for the last four millennia during which time growth rates were high and $\delta^{13}C$ values were low in response to wetter conditions. The regional Aridity Index documents that Middle Holocene drying coincided with a warm Arctic and decreased sea ice extent, a warm western tropical Pacific, and a large sea surface temperature gradient across the tropical Pacific, all of which likely responded to northern hemisphere summer insolation forcing. Our data suggest that extreme Middle Holocene aridity is more severe than the short medieval droughts evident in the tree ring record, and such extreme aridity may represent a worst-case analog for future climate.

1. Introduction

1.1. Modern Controls on Southwestern Aridity

There is a compelling need for a precise understanding of the drivers of Holocene hydroclimatic variability in the southwestern United States (hereafter "the Southwest," comprising Arizona, Nevada, New Mexico, and the southern tiers of California, Utah, and Colorado), to guide policies and to respond to anthropogenic climate change (Cook et al., 2015). For the modern period, climate dynamical studies have demonstrated that Southwestern drought is linked to warming in western tropical Pacific sea surface temperature (SST) and warming in the Arctic (Routson et al., 2019; Swain et al., 2017), both of which are associated with a strengthened north Pacific subtropical high-pressure cell and reduced midlatitude winter precipitation (Cvijanovic et al., 2017; Kirby et al., 2015; Meehl & Hu, 2006; Seager et al., 2015; Sewall, 2005; Swain et al., 2017). Although there remains uncertainty in whether reduced Arctic sea ice forces an atmospheric response in the northeast Pacific (Cohen et al., 2020; Overland et al., 2016; Swain et al., 2017), observational evidence suggests that pan-Arctic warming is associated with warmer winter temperatures in Western North America (Cohen et al., 2020) connected to changes in the Siberian High and/or sea-ice conditions. Midlatitude Pacific and Atlantic SSTs have also been linked to Southwestern drought variability (Aziz et al., 2010; Oglesby et al., 2012). While recent changes in Southwest precipitation have been associated with pronounced ridging and high pressure in the northeast Pacific arising from teleconnections to tropical Pacific warming and sea ice decrease in the Barents and Kara Seas (Swain et al., 2017), the degree to which these remote teleconnections may affect climate, if at all, over the Holocene Epoch remains less clear, thereby impeding our ability to project long-term future changes in this water-limited region. A large concern is that rising greenhouse gas concentrations and associated climate responses may result in a change in the Southwest's climate toward long-term aridification in the Southwest (Cook et al., 2015), with implications for sustaining human populations reliant on water resources in this arid region.

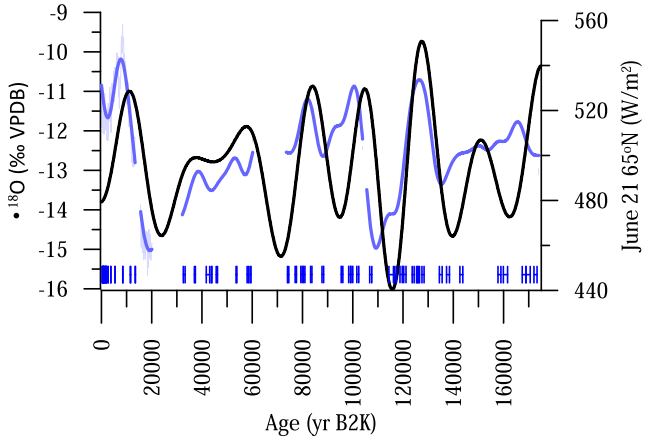

Figure 1. Leviathan Cave $\delta^{18}O$ variations over the last 175,000 yr track northern hemisphere summer insolation (21 June). These data show that summer insolation is a prime forcing on Great Basin paleoclimate on orbital time scales but that the $\delta^{18}O_{ivc}$ values lag NHSI by >3,000 yr on average. Data from Lachniet et al. (2017). Bold blue curve is a zero-phase Butterworth filter. U-series ages are shown with the bars on the bottom plot; hiatuses are represented by breaks in the time series.

The challenge of potential future aridification in the Southwest is highlighted by observed decreases in the water supply in the highly engineered Colorado River and Rio Grande basins, which are critical human support systems as their headwaters in the Rocky Mountains supply snow-fed water for myriad economic uses and support 56 million residents (Garfin et al., 2013). A water supply/allocation imbalance in the Colorado River Basin has heightened socioeconomic sensitivity to drought (Fleck, 2016), as witnessed in the recent drought that began in 2001 and has resulted in historic low reservoir levels in Lake Mead. This drought was registered amid detected trends of decreased snowpack and Colorado River flow (Mote et al., 2018; Woodhouse et al., 2016), and climate projections suggest a hotter and drier Southwest (Seager & Vecchi, 2010) that will exacerbate water limitation. Of particular concern to water supply are "hot droughts" (Udall & Overpeck, 2017), which arise when anomalous warmth and drying amplify water shortages. Anthropogenic warming of the climate system may make hot droughts more common, as the Southwest is expected to dry because of increased evaporative demand (Ault et al., 2016), a likely northward shift of storm tracks (Salathé, 2006), and decreased snow pack, Colorado River streamflow, and soil moisture (Cook et al., 2015; Fyfe et al., 2017; Seager & Vecchi, 2010; Udall & Overpeck, 2017; Woodhouse et al., 2016). Recent results point to increased aridification because of an increase in evaporative demand due to warmer conditions, even if precipitation remains the same or increases (Williams et al., 2020).

1.2. Aridity Constraints From Paleoclimatic Data

Paleoclimate data allow understanding of the past behavior of climate on timescales longer than the instrumental record. The paleoclimate perspective on Southwestern drought over the last few millennia is provided primarily from tree-ring records, which revealed that decadal- to centennial-scale droughts were common features of natural climate variability (Cook et al., 2010; Meko et al., 2007; Williams et al., 2020; Woodhouse et al., 2010). For example, during Medieval time (CE 800–1300) there was widespread drought on the Colorado Plateau and Sierra Nevada (Cook et al., 2010). For the upper Colorado River Basin, the ten year drought between 1146 and 1155 was selected as a "worst case" future analog drought (Woodhouse et al., 2010). These so-called Medieval "megadroughts" have been attributed to a La Niña-like climate state in the tropical Pacific Ocean (Graham et al., 2007; Routson et al., 2011; Williams et al., 2020; Woodhouse et al., 2010) or to stochastic variability (Coats et al., 2016). However, only a few dendroclimatic records extend beyond the past two millennia (Millar et al., 2018; Salzer et al., 2014) and may not fully represent a long-term shift towards a more arid climate state because they do not extend through the Middle Holocene.

Previous work on the Nevada speleothem (cave calcite) record indicated a strong orbital signal in the temperature-sensitive $\delta^{18}O$ data (Lachniet et al., 2014, 2017). On orbital timescales (Figure 1), Nevada speleothem data show that Great Basin climate exhibited a one-to-one correlation with northern hemisphere summer insolation (NHSI) on June 21, with a temporal lag that averaged 3,240 yr (Lachniet, 2016; Lachniet et al., 2014, 2017). The strong orbital character of the Leviathan Cave and Lehman Caves composite record (Figure 1) is evident from the strong visual similarity to northern hemisphere summer insolation at 65°N. Other Holocene $\delta^{18}O$ speleothem records from Lehman Caves do not show this strong orbital character (Steponaitis et al., 2015), suggesting that their response to northern hemisphere paleoclimate is registered differently than in our records. The lagged relationship between Leviathan Chronology $\delta^{18}O$ and insolation was suggested to have arisen through the indirect forcing of changes in the Arctic cryosphere, because of its relatively fast response to northern hemisphere temperature and insolation (Lachniet et al., 2014, 2017). A direct precipitation $\delta^{18}O$ response in the Great Basin to insolation variation is less likely because peak $\delta^{18}O$ at ~8,400 yr B2K was reached several thousand years after the ~11,000 yr B2k insolation peak.

However, the previous work focused only the significance of the orbital-scale $\delta^{18}O$ variations and did not investigate the sub-orbital structure of Holocene temperature and aridity evolution, the timescale of Holocene climatic change, or possible links to the Pacific Ocean. The lower resolution isotope data

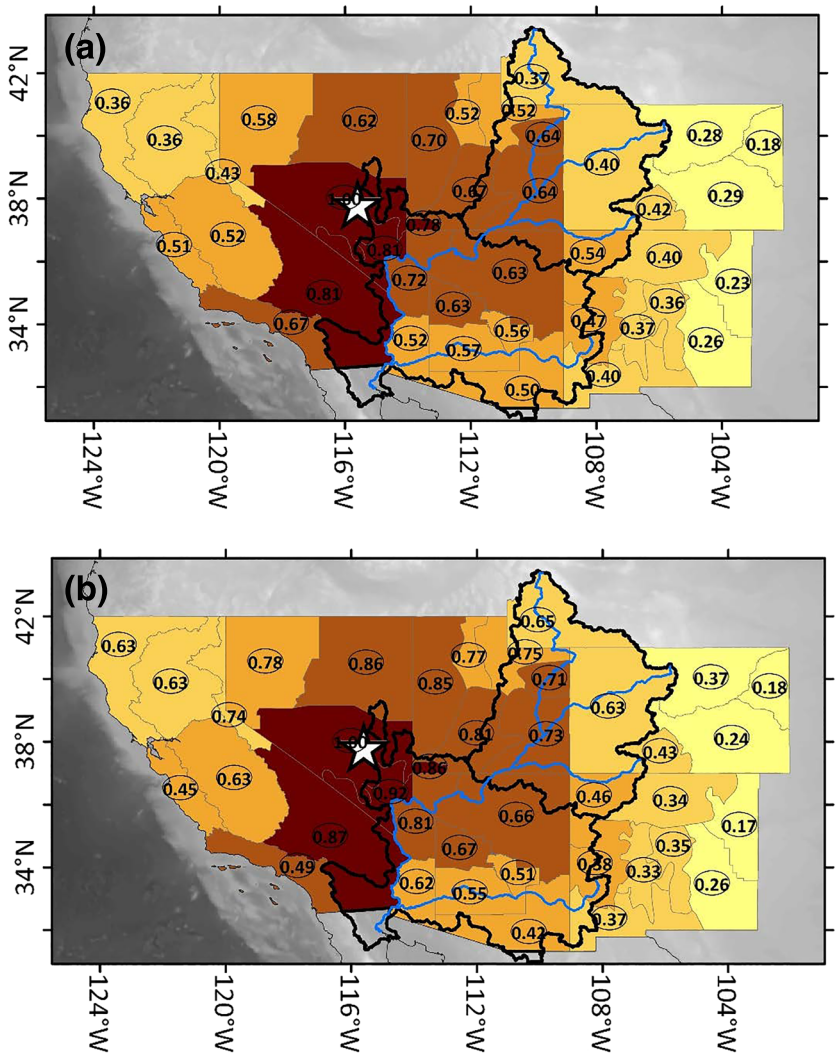

Figure 2. Correlations between climate divisional data (1895–2015) for (a) Palmer drought severity index and (b) Max annual temperature, between the climate division containing Leviathan Cave (white star) and other regional divisions. For PDSI, the strongest correlations are found for the climate division containing the Sierra Nevada ($R = 0.81$), southern California ($R = 0.67$), and along the Colorado River corridor in the upper and lower basins ($R > 0.5$ to 0.8; thick black polygons). Maximum temperature correlations exceed $R > 0.8$ along the entire lower Colorado River Basin and $R > 0.63$ for the upper Colorado River, suggesting that the Leviathan Cave record should be representative for the broader southwestern United States.

previously presented may have also missed large-magnitude climate shifts operating on sub-centennial timescales, a possibility that we can now assess with our new decadal resolution data. As such, the potential controls on the Holocene climate evolution in the Leviathan Cave record or the broader Southwest more generally have not yet been investigated in sufficient detail to test for other potential forcings. Further, a compilation of additional moisture-sensitive proxy data, as we present below, will assist in evaluating the spatial extent of Holocene hydroclimate variations.

Among the records in our Aridity Index, many document the presence of Middle Holocene dry intervals as inferred from lake sediment, pollen, and packrat records at sites across the western United States (Bartlein et al., 2014). These sites include the Great Basin and Sierra Nevada (Grayson, 2011; Harrison et al., 2003; MacDonald et al., 2016; Thompson et al., 1993), Mojave Desert (Kirby et al., 2015; Wigand & Rhode, 2002), Great Basin desert (Shuman et al., 2010), Sonoran Desert (Blinn et al., 1994), and Rocky Mountains (Shuman & Serravezza, 2017). For the Sierra Nevada, the Middle Holocene aridity was

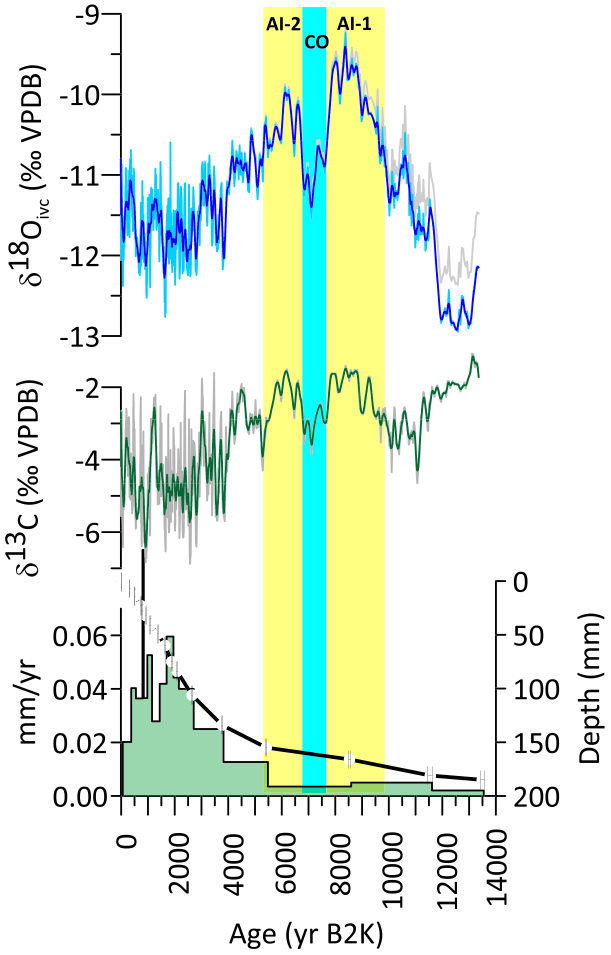

Figure 3. High-resolution stable isotope values, U-series ages, and growth rate for stalagmite LC-1. The $\delta^{18}O_{ivc}$ and $\delta^{13}C$ values (thin blue and green lines) are shown with a 101-yr running averages (thick lines). Thin gray line is measured $\delta^{18}O$ values before ice-volume correction. U-series ages show 2-σ uncertainties. Growth rate was slow until it increased dramatically in the late Holocene. Aridity intervals 1 and 2 (AI-1 and AI-2) are shown in yellow bars, and the Cool Oscillation (CO) in blue.

attributed to changes in Pacific Ocean sea surface temperature (Kirby et al., 2015; MacDonald et al., 2016) analogous to persistent La Niña-like conditions with a cool east and warm western tropical Pacific and to establishment of modern boundary conditions following retreat of the Laurentide Ice Sheet. Additionally, a time-slice comparison between 6 ka and modern against model output suggests that atmospheric ridging reduced the amount of winter precipitation reaching much of the western United States during the Middle Holocene, and regions near the U.S. Southwest/Mexico border were wetter because of an enhanced summer rainfall contribution (Hermann et al., 2018). Further, analysis of North American pollen data suggests long-term warming throughout the Holocene, reaching near-modern levels at around 7,000 yr BP with only a slight decrease to the modern (Marsicek et al., 2018) in a manner that is inconsistent with an NHSI periodicity and the 175,000 yr long Leviathan speleothem record (Lachniet, 2016; Lachniet et al., 2014, 2017).

1.3. Study Area and Climate

Leviathan Cave (37.89°N, 115.58°W, 2,400 m) is located in the Worthington Mountain Wilderness in Basin and Range National Monument in central Nevada and is part of the southern Great Basin. The precipitation seasonality for the study area is representative of the broader Pacific Southwest, Great Basin, and lower Colorado River Basin and is dominated by winter precipitation delivered by synoptic storm systems (Cayan & Roads, 1984; Hereford et al., 2006; Seager & Vecchi, 2010), which are sometimes concentrated into narrow but concentrated bands of moisture known as atmospheric rivers (Dettinger, 2013; Gershunov et al., 2017). Summer precipitation from the North American Monsoon that reaches the cave site arises almost entirely from the Gulf of California. Gulf of Mexico moisture rarely reaches the Great Basin but does substantially contribute to rainfall in Arizona, New Mexico, Utah, and Colorado (Jana et al., 2018). While summer monsoon moisture is a significant contributor to annual precipitation totals in some areas, particularly in the Sonoran and Chihuahuan Deserts of Arizona and New Mexico (Hereford et al., 2006), it typically does not contribute to groundwater infiltration in the Great Basin (Winograd et al., 1998) or to streamflow in the Upper Colorado River Basin (Serreze et al., 1999).

To test for the spatial correlation structure between our site and the broader Southwest, we correlated annual climate data for the Leviathan Cave climate division (Nevada climate division 3) against Pacific Southwest divisions (Figure 2) between 1895 and 2015. This comparison shows that the Leviathan Cave region is representative of climate conditions in most of the Mojave Desert and southern Great Basin, with Pearson R correlations of around 0.7 to 0.8 for Palmer Drought Severity Index values and 0.8 to 0.9 for maximum temperature between divisions. The study area is also modestly correlated in PDSI to the lower (R ~0.5 to 0.7) and upper (R ~0.4 to 0.65) and Colorado River basins (Figure 2). These data show that the drought and temperature signature of modern climate variability shares similarity between our study area and the broader Pacific Southwest, such that our data have implications for the broader desert region.

2. Methods

Holocene paleoclimate in stalagmite LC-1 is constrained by 840 $\delta^{18}O$ and $\delta^{13}C$ values, with subsampling at a higher resolution than previous publications (Lachniet et al., 2017). Stalagmite LC-1 from Leviathan Cave, Nevada was milled at 0.1 to 0.2 mm intervals over the uppermost 85 mm depth, drilled at 0.5 mm resolution between 85 and 154 mm, milled at 0.25 mm resolution between 154 and 171.75 mm, and milled at 0.1 mm intervals between 171.75 and 184.75 mm, providing temporal resolution of <5 to ~60 yr (Figure 3). $\delta^{18}O$ and

$\delta^{13}C$ values were determined on a Kiel IV carbonate device via phosphoric acid digestion at 70°C and analyzed on a Delta V Plus dual inlet mass spectrometer. Isotopic values were calibrated against an in-house internal standard that was calibrated to international standards NBS-18 and NBS-19 in a two-point calibration; mean precision for $\delta^{18}O$ and $\delta^{13}C$ is 0.08‰ and 0.06‰, respectively. We corrected $\delta^{18}O$ values for ice volume-driven changes in ocean water $\delta^{18}O$ by subtracting changes in ocean water $\delta^{18}O$ values from the reconstruction of Waelbroeck et al. (2002), denoted here as $\delta^{18}O_{ivc}$ (Figure 3). The magnitude of this correction is small (<0.7‰ at the Younger Dryas [YD], tapering to 0‰ for the modern) and has no effect on the interpretations of the data. Water $\delta^{18}O$ and $\delta^{2}H$ values were determined on a high-temperature thermal conversion elemental analyzer (TC/EA) via pyrolysis at 1,400°C in the presence of glassy carbon and analyzed via continuous flow on a ConFlo III device. Values were calibrated to internal standards that were calibrated to international standards; mean precision for $\delta^{18}O$ and $\delta^{2}H$ is 0.2‰ and 2.0‰, respectively. All stable isotope determinations were made at the Las Vegas Isotope Science Lab at the University of Nevada Las Vegas. Ages were determined at the University of New Mexico Radiogenic Isotope Laboratory, reported as years before the year 2000 CE (yr B2k). For the Holocene section of LC-1, 16 U-series ages are all in stratigraphic order. The high precision (2 σ age uncertainties are better than $\pm$ 96 yr) of the U-series ages is a result of high uranium concentrations and initial $\delta^{234}U$ values (>1,900‰). The age model consists of linear fits to the U-series age/depth relationships, and additional details of the age modeling for stalagmite LC-1 were previously reported (Lachniet et al., 2014).

3. Results

Leviathan Cave today has constant 100% relative humidity in the sampling room and constant temperature of 8.32 $\pm$ 0.06°C, making an ideal environment in which calcite $\delta^{18}O$ values appear to have been deposited in apparent isotopic equilibrium with cave drip waters (Lachniet et al., 2014). Seven pool water samples fed from drips in Leviathan Cave were collected in 2011, 2012, and 2013 and have $\delta^{18}O$ values of −14.0‰, −14.2‰, −13.0‰, −13.0‰, −13.6‰, −13.3‰, and −13.2‰ VSMOW, with corresponding deuterium excess values of 8.8, 9.2, 5.3, 2.5, 8.0, 11.1, and 9.0. The uppermost LC-1 $\delta^{18}O$ value is −10.8‰ VPDB. At the measured cave temperature of 8.32°C, this calcite would be in apparent isotopic equilibrium with drip water values of −13.66‰ VSMOW (Daëron et al., 2019) or −13.59‰ VSMOW (Coplen, 2007), nearly the same as the measured pool water samples. Comparison of the pool waters and cave drip water to seasonal precipitation $\delta^{18}O$ values suggests that the infiltration is dominated by winter precipitation, as is most recharge in the Great Basin (Winograd et al., 1998). We conclude that summer rainfall does not currently make a significant contribution to rechargeat our cave site, though it may have contributed in the past if summer precipitation amounts were higher.

Stalagmite LC-1 $\delta^{18}O_{ivc}$ values (in ‰ VPDB) range from a low of −12.95‰ during the Younger Dryas (12,580 yr B2K) to a max of −9.24‰ (8,380 yr B2k) (Figure 3; Data Set S1). The post-YD $\delta^{18}O$ increase was punctuated by two abrupt "overshoots" at 11,550 yr B2k and 10,580 yr B2k. The transition out of the YD occurred over 3,400 yr. Following peak $\delta^{18}O$ values at ~8,400 yr B2k, an abrupt negative $\delta^{18}O$ anomaly between 7,740 and 6,730 yr B2k is superimposed on a more gradual $\delta^{18}O$ decrease that reaches near-modern levels at ~4,000 yr B2k. From 4,000 yr B2k to the modern, $\delta^{18}O$ values vary between −12.5‰ and −11.0‰. Since ca. 1,600 yr B2k, $\delta^{18}O$ values show a tendency to increasing values. Carbon stable isotopes provide complementary isotopic data. $\delta^{13}C$ values were high (approximately −2‰) during the YD and remained between −2‰ and −4‰ between the YD and the end of the Middle Holocene after which time the mean value decreased to between −4‰ and −6‰. The last 4,000 yr of stalagmite growth also show abrupt $\delta^{13}C$ variability about the mean but do not show any $\delta^{18}O$ or $\delta^{13}C$ high extremes that exceed the variability in the Early and Middle Holocene.

3.1. Precipitation Isotope Constraints on Interpretation of Stalagmite $\delta^{18}O$

To determine the controls on modern precipitation $\delta^{18}O$ values and assist in the interpretation of speleothem $\delta^{18}O_{ivc}$, we analyzed the relationship between precipitation $\delta^{18}O$ values and temperature, precipitation amount, and moisture source on 233 precipitation samples over 98 precipitation days collected in Southern Nevada between 2007 and 2017 (Data set S2). Most of the samples were "grab" samples at the sub-event scale in the Las Vegas Valley, but some represent full integrated precipitation events. The Local

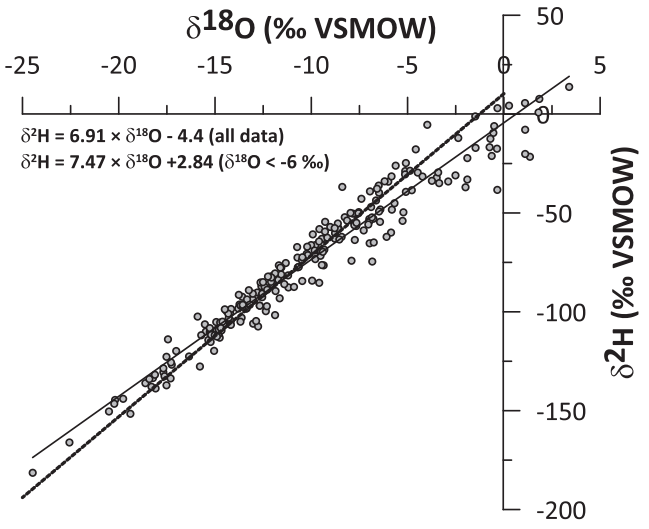

Figure 4. Southern Nevada Meteoric Water Line, $\delta^{18}O$ values in southern Nevada span a range of nearly 30‰. The full data set define a local meteoric water line that has a lower slope and intercept compared to the Global Meteoric Water Line, indicating some evaporation of samples. If the LMWL is based only on samples with $\delta^{18}O$ values ≤6‰, the slope is 7.47 and the intercept is +2.84. Dotted line is the Global Meteoric Water Line ($\delta^2H = 8.17 \times \delta^{18}O + 10.35$).

Meteoric Water Line (LMWL; Figure 4) is defined as $\delta^2H = 6.9 * \delta^{18}O - 4.4$, and $\delta^{18}O$ values span nearly 30‰. The relatively low slope and intercept indicate evaporation of some samples in the sub-cloud environment. The meteoric water line determined on samples with $\delta^{18}O$ values of less than −6‰ (approximately the summer/winter cutoff) is $\delta^2H = 7.47 * \delta^{18}O + 2.84$, which has a lower slope and intercept than the Global Meteoric Water Line of $\delta^2H = 8.17 * \delta^{18}O + 10.35$ (Rozanski et al., 1993); the intercept of 2.84 also indicates the possibility of some sub-cloud evaporation. Histograms of seasonal rainfall show highest values in the summer (June through October; −4.7 ± 3.8‰) and lowest values in the winter (November through May, −12.3 ± 4.1‰; Figure 5).

To test the relationship between precipitation $\delta^{18}O$ and temperature, we show an analysis that used winter precipitation data from 19 sites across the Great Basin (Friedman, 2002), previously reported in Lachniet et al. (2014). Winter amount-weighted precipitation $\delta^{18}O$ values are strongly correlated to mean winter temperatures ($r^2 = 0.68$, $p < .000005$) but not significantly correlated to rainfall amount ($r^2 = -0.12$, $p = 0.14$). These data (Figure 6a) demonstrate that Great Basin winter precipitation is strongly related to site temperature on a spatial basis. Next, we used the weather type classification of Sheridan (Sheridan, 2002) to assign each precipitation sample in our southern Nevada data set to a synoptic type and determined daily maximum, mean, and minimum surface air temperatures (in °C) and precipitation amount (mm) from the KLAS station (36.08°N, 115.16°W, 659 m asl). The synoptic types are related to moisture source, with polar, midlatitude ("moderate"), and low-latitude ("tropical") origins. The synoptic weather types with the most total cumulative precipitation (Table 1) in our data set are, in descending order, Moist Moderate, Transition, Moist Tropical, Moist Polar, Dry Moderate, and Dry Polar and Dry Tropical. The latter two types in our data set are represented by only trace amounts. Most of the precipitation was generated in the Moist Moderate type, which is characterized by a midlatitude moisture source over the Pacific Ocean or Gulf of California. Moist Polar is associated with precipitation events resulting from transport of high-latitude moisture to the Great Basin and is also a winter type. The Moist Tropical weather type is characterized by low-latitude north Pacific moisture and is most common in October (end of the summer monsoon season) and November (beginning of the winter). There is not a specific event type associated with the summer monsoonal rains in our study area, with Moist Moderate, Dry Moderate, and Moist Tropical being the most common. We did not observe a clear relationship between $\delta^{18}O$ values and atmospheric rivers in our data set (not shown), a finding similar to that of a precipitation isotope study upwind in California (McCabe-Glynn et al., 2016).

We show that there is also a strong control between moisture source, mean daily temperature of precipitation events, and $\delta^{18}O$ values in Figure 6b. Precipitation derived from the North Pacific (Moist Polar weather type) tends to be coldest (9.2 ± 5.5 °C) and with lowest $\delta^{18}O$ values (−14.8 ± 5.8‰). The Moist Moderate event type is warmer (10.9 ± 5.5 °C) and has intermediate $\delta^{18}O$ values (−11.9 ± 4.0‰). The transitional type is similar to the Moist Moderate type with only slightly higher $\delta^{18}O$ ($\delta^{18}O = -11.0 \pm 4.9$‰ and mean temperature = 11.9 ± 6.1 °C). Highest $\delta^{18}O$ values are associated with the Moist Tropical type (−5.5 ± 5.3‰), which also has the highest temperatures of the "moist" types (19.7 ± 7.7 °C). It is clear from Figure 6 that lowest $\delta^{18}O$ values indicate both a middle- to high-latitude moisture source and low temperatures and vice versa for low latitude and summer moisture sources. The $\delta^{18}O$ in Figure 6b is strongly correlated with mean daily temperature of synoptic types, defined by an equation of $\delta^{18}O = 0.40 \times Tmean - 15.98$ ($r^2 = 0.76$, $p < .05$). Snow typically has the lowest values, in our data set ranging from −12.7‰ to −22.6‰ VSMOW ($n = 9$) spanning the lower end of the winter $\delta^{18}O$ distributions (Figure 4) and very different from summer monsoon values ($\delta^{18}O = -4.7 \pm 3.8$‰; Figure 5).

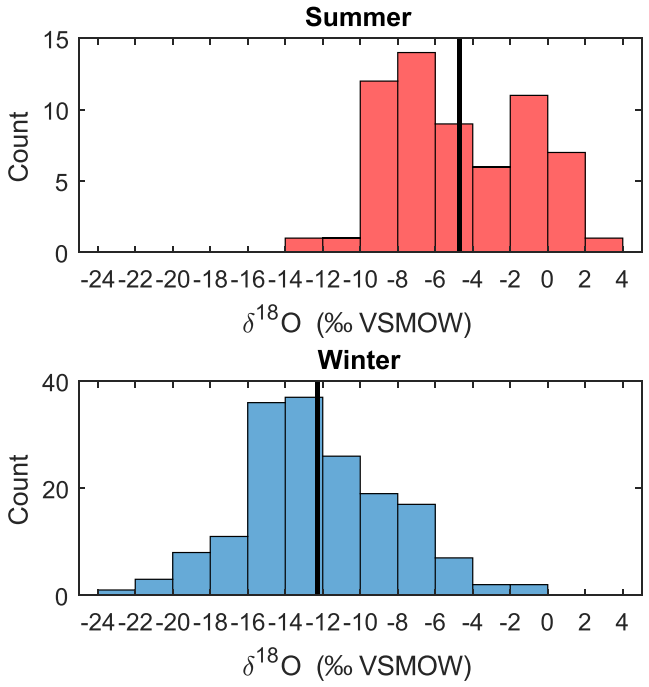

Figure 5. Summer and winter precipitation $\delta^{18}O$ histograms for Las Vegas. The precipitation $\delta^{18}O$ data show higher values in the summer and lower in the winter. The drip and pool waters in Leviathan Cave, located at ~1,400 m altitude of ~−14 ‰ are consistent with a dominant source from winter precipitation.

3.2. Stalagmite Proxy Interpretation

This isotope climatology analysis (Figures 5 and 6) provides strong support for the interpretation of precipitation $\delta^{18}O$ as a proxy for covariable moisture source and air temperatures. Further, because modern Leviathan Cave drip waters are dominated by winter snowmelt (Lachniet et al., 2014), stalagmite LC-1 ice-volume corrected oxygen isotopes ($\delta^{18}O_{ivc}$) are interpreted primarily as a proxy for winter moisture source and temperature. Because observed snow $\delta^{18}O$ values are lower than rain for a given storm, a change from more to less snow during winter would also be expected to result in higher drip water $\delta^{18}O$ values. We interpret the $\delta^{13}C$ values in the stalagmite as an effective moisture proxy, possibly modified by moisture-limited kinetic isotope effects, because there is a positive correlation between Great Basin soil pedogenic carbonate $\delta^{13}C$ values and effective moisture (Amundson et al., 1988; Quade et al., 1989). These studies demonstrated that soil CO_2 has lower $\delta^{13}C$ values in wetter conditions, because of enhanced plant respiration of isotopically light carbon, and this $\delta^{13}C$ signal should also be imparted into percolating soil waters that eventually reach the cave and speleothem calcite. Further support for an effective moisture control on stalagmite $\delta^{13}C$ values is evident in the strong correlation between high stalagmite growth rates and low speleothem $\delta^{13}C$ values ($r^2 = 0.65$) (Lachniet et al., 2014). Higher stalagmite growth rates are thus interpreted to relate to enhanced cave drip water CO_2 concentrations and higher bicarbonate concentrations, and wetter periods are characterized by lower $\delta^{13}C$ values of dissolved inorganic carbon in soil waters infiltrating into caves. Because stalagmite $\delta^{13}C$ values and growth rates may have multiple forcings other than effective moisture (Fairchild & Baker, 2012; Wong & Breecker, 2015), we consider them qualitatively. Because we are unable to unambiguously constrain precipitation amounts from the speleothem isotopic data, we have also compiled an Aridity Index that constrains effective moisture variations over the Great Basin and broader Southwest region (detailed below).

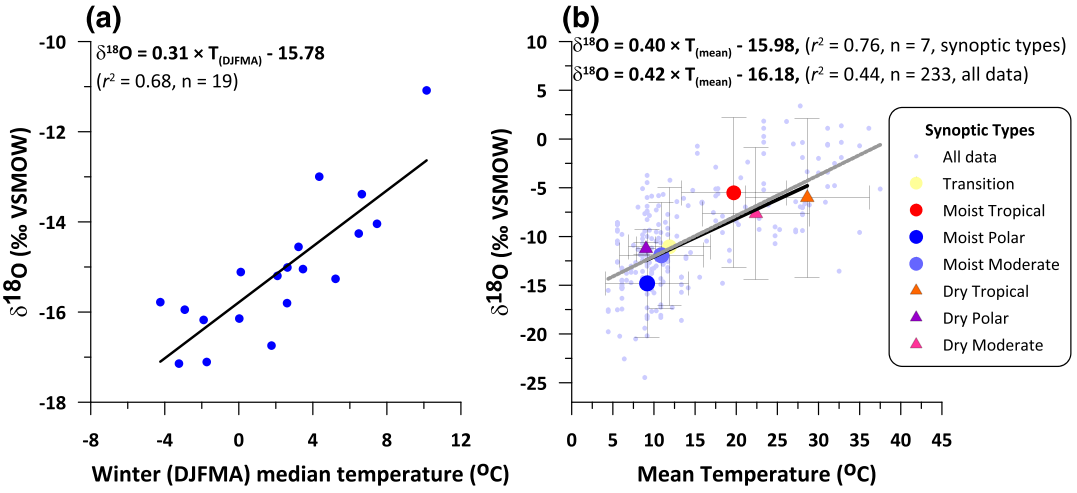

Figure 6. Nevada precipitation $\delta^{18}O$ values are correlated to temperature and moisture source. (a) shows the correlation between winter $\delta^{18}O$ and temperature in stations around the Great Basin (Friedman, 2002), demonstrating that winter $\delta^{18}O$ values are strongly correlated to temperature. (b) shows that southern Nevada precipitation $\delta^{18}O$ values from Las Vegas are also strongly related to mean event temperature and moisture source, with higher latitude synoptic weather types associated with lower $\delta^{18}O$ values and lower temperature, and vice versa.

Table 1
Stable Isotope and Climate Paramaters for Synoptic Weather Types Around Las Vegas, Nevada

Synoptic weather type	Mean $\delta^{18}O$ (‰ VSMOW)		Mean $\delta^{2}H$ (‰ VSMOW)		Mean dx		Count	Mean max T (°C)		Mean min T (°C)		Mean mean T (°C)		Mean precip (mm)		Sum precip (mm)
Dry moderate	−7.7	±4.6	−55	±35	5.9	±9.8	20	27.7	±7.0	17.1	±6.5	22.4	±6.7	4.5	±5.8	90
Dry polar	−11.3	±2.0	−83	±20	7.1	±3.6	2	13.9	±0.0	4.2	±1.2	9.0	±0.6	Trace	Trace	Trace
Dry tropical	−6.0	±3.5	−49	±23	−1.1	±14.8	10	34.7	±8.9	22.6	±7.5	28.6	±8.2	0.3	±0.4	3
Moist moderate	−11.9	±4.0	−86	±31	9.8	±6.9	132	13.4	±5.9	8.4	±5.1	10.9	±5.5	10.5	±9.0	1,381
Moist polar	−14.8	±5.8	−108	±39	10.0	±9.6	9	12.4	±6.1	5.9	±5.0	9.2	±5.5	4.0	±7.9	36
Moist tropical	−5.5	±5.3	−44	±35	0.7	±13.1	31	23.6	±9.2	15.8	±6.4	19.7	±7.7	5.5	±4.4	171
Transition	−11.0	±4.9	−84	±33	4.2	±7.9	24	15.1	±7.3	8.6	±5.0	11.9	±6.1	7.2	±6.2	174

Because of the strong orbital character of the speleothem record, the high dating precision, continuity, and high-resolution stable isotope and growth rate data from stalagmite LC-1, we consider the Leviathan Cave record as a robust record of paleoclimate in the central and southern Great Basin. The strong correlations between modern PDSI and temperature between the Leviathan Cave climate division and other divisions in the Mojave Desert and southern Great Basin (Figure 2) suggest that it is likely to be representative of paleoclimatic conditions there. Further, our record has moderate correlations that extend (somewhat less strongly) into Arizona, southern Utah, and western Colorado, suggesting that our results may also be representative of the broader Southwest in general and the Colorado River Basin in particular.

3.3. Great Basin Paleoclimate Since the Younger Dryas

The details of the Holocene Leviathan Cave record reveal several distinct climate shifts over time. We interpret the sustained low $\delta^{18}O_{ivc}$ values during the Younger Dryas to indicate cool conditions relative to the early Holocene (Figure 3) associated with the ~4°C cooler sea surface temperature estimates from the northeast Pacific Ocean (Barron et al., 2003). High $\delta^{13}C$ values and slow growth during the Younger Dryas are consistent with the hypothesis of low soil productivity, which is plausibly linked to arid conditions. These data conflict with interpretations of wetness in southern (Quade et al., 1998) and north Central Nevada (Huckleberry et al., 2001). This apparent discrepancy may reflect increased recharge and less evaporation during periods of lower temperature, allowing for aquifer recharge in southern Nevada or a lag time of regional groundwater discharge to climate changes.

Most prominently, the $\delta^{18}O_{ivc}$ data show a gradual increase, reflecting warming or a change to a more southerly moisture source after 11,700 yr B2k to reach peak warmth at 8,380 yr B2k (Figure 3). The 2,180 yr interval between 9,850 and 7,670 yr B2k coincided with high $\delta^{18}O_{ivc}$, high $\delta^{13}C$, and slow growth rates, reflecting the warmest and driest Holocene period. We term this Aridity Interval 1 (AI1), and it is defined by $\delta^{18}O_{ivc}$ values above a threshold of −10.77‰, the peak value of a 101-yr moving average over the last 4,150 yr. Of note, we observed no indication of a climate anomaly associated with the so-called 8.2 ka event (Alley & Agustsdottir, 2005), and winter precipitation in the Great Basin appears not to have been affected at this time, which stands in contrast with the supposition of a winter climate perturbation at this time upstream in the Sierra Nevada (Oster et al., 2017). After a 900 yr-long cool oscillation between 7,670 and 6,770 yr B2k, a second Aridity Interval (AI2) endured for 1,460 yr between 6,770 and 5,310 yr B2k. Our observations of the two aridity intervals attest to the extreme dry Early to Middle Holocene climate state in the Great Basin.

The peak $\delta^{18}O_{ivc}$ value of ~−9.5‰ VPDB in the Middle Holocene corresponds to a drip water $\delta^{18}O$ value of −12.4‰ VSMOW at modern temperature of 8.32°C or −11.9 ‰ VSMOW with 2°C warming above modern levels using the most-recent calcite-water fractionation factor for slow-growing speleothems (Daëron et al., 2019). The estimated paleo-drip water $\delta^{18}O$ values of −11.9‰ to −12.4‰ VSMOW are the essentially the same as the modern winter precipitation value in southern Nevada (Las Vegas) of −12.3 ± 4.1‰ VSMOW, from a location that is slightly warmer and lower altitude than Leviathan Cave. In contrast, the estimated paleo-drip water $\delta^{18}O$ values do not overlap with a summer monsoon signature (Figure 5). A contribution to cave recharge of a larger than normal proportion of summer precipitation may have contributed to the peak $\delta^{18}O_{ivc}$ values, an idea consistent with data supporting an increase in the strength of the summer

monsoon (Diffenbaugh et al., 2006; Metcalfe et al., 2015). However, a large contribution can be ruled out because the estimated paleo-drip water values of around −12‰ VSMOW are within the normal winter precipitation $\delta^{18}O$ range (−12.3 ± 4.1 ‰ VSMOW). The simplest interpretation of the peak $\delta^{18}O_{ivc}$ value is that during the Middle Holocene there was more winter moisture from middle- to low-latitude moisture sources, such as the Moist Moderate and Moist Tropical sources, while the high $\delta^{13}C$ values indicate drier conditions.

In the Late Holocene, $\delta^{18}O$ and $\delta^{13}C$ values decrease while growth rate increases, with a sudden step change at around 4,200 yr B2k to apparently wetter and cooler conditions. Our data are consistent with the observation that a warm and arid Middle Holocene was followed by a wetter and cooler Late Holocene nearly everywhere in the broader Southwest (Grayson, 2011; Kirby et al., 2015; MacDonald et al., 2016; Polyak & Asmerom, 2001; Thompson et al., 1993). This interval corresponds to the "Neopluvial" in the Bonneville Basin when lake levels began transgressing at ca. 5,000 yr B2k, and our record indicates a decrease in $\delta^{13}C$ values and an increase in growth rate, substantiating both our interpretations of the stalagmite growth rate and $\delta^{13}C$ as proxies for effective moisture and interpretations of beach geomorphology in the Bonneville Basin reflecting lake high stands (Madsen, 2000).

3.4. An Aridity Index Indicates the Broad Spatial Scale of Middle Holocene Aridity

There is abundant regional evidence that shows warmer and drier conditions during the Middle Holocene in Western North America (Bartlein et al., 2014) and the Great Basin and Sierra Nevada (Grayson, 2011). For example, the Bonneville Basin experienced peak aridity ~8,500 yr B2k (Louderback & Rhode, 2009), coincident with peak Holocene temperatures (Madsen & Currey, 1979). The magnitude of this arid interval is suggested by sedimentary evidence from the Great Salt Lake suggestive of complete desiccation (Madsen, 2000). Sub-fossil trees from the White Mountains on the Nevada/California boundary (LaMarche, 1973) also document a 150 m rise in tree line at ~8,300 yr B2k likely due to climatic warming. A similar observation of a 68 m tree line rise in the Sierra Nevada was documented for Foxtail pine between ca. 7,200 and 3,900 yr B2k (Scuderi, 1987). Hydrogen isotope (δD) variations in Bristlecone pines on the White Mountains document peak values at 6,800 yr B2k, highest of the 8,000 to 4,100 yr B2k interval (Feng & Epstein, 1994), interpreted to represent conditions warmer than today. Tree stumps submerged in Lake Tahoe document lake levels 5 to 12 m below the natural sill level by between 6,300 and 4,800 yr B2k (Lindström, 1990), and the now-drained Tulare Lake in the Central Valley of California was also at low levels between 7,800 and 4,500 yr B2k (Davis, 1999). Owens Lake contains a sediment hiatus between ca. 6,700 and 4,500 yr B2k on core OL84b (Benson et al., 1997) or between 5,800 and 9,300 yr B2k on core OL-92 (Bischoff et al., 1997), and low stands between 6,900 and 4,350 yr B2k (Bacon et al., 2006), attributed to arid conditions. Pollen data from Pyramid Lake indicate driest conditions of the Holocene between 7,600 and 6,300 yr B2k (Mensing et al., 2004) and lowest levels between ca. 8,000 and 4,800 yr B2k (Adams & Rhodes, 2019). In the Sierra Nevada, meadow sediments document dry mid-Holocene conditions (Anderson & Smith, 1994), pollen data show a warmer and drier climate prior to 6,800 yr B2k (Anderson, 1990), and peak fire occurrence rates mark the period ca. 8,000 and 3,800 yr B2k when tree lines were higher than today (Hallett & Anderson, 2010). In southern Nevada (Las Vegas Valley), spring-fed marshes largely dried up around 8,000 yr B2k and were replaced with eolian deposits (Quade, 1986). Diamond Pond in southeastern Oregon was 17 m lower than modern prior to 6,200 yr B2k, when a saline-soil adapted biota (greasewood) dominated the pollen spectra (Wigand, 1987). The xerophytic creosote bush was at highest concentrations during the mid-Holocene between ca. 7,700 and 5,800 yr B2k in southern Nevada, and species diversity was lowest in packrat middens relative to the late Holocene (Spaulding, 1991). The Ruby Marshes in northeast Nevada showed slowest sedimentation rates between 8,000 and 5,100 yr B2k, suggesting arid conditions (Thompson, 1992), and the Blue Lake meadows on the western margin of Lake Bonneville largely dried between 8,300 and 6,500 yr B2k (Louderback & Rhode, 2009). Stonehouse Meadow in northern Spring Valley was restricted or absent prior to 8,000 yr B2k and began expanding after 7,500 yr B2k (Mensing et al., 2013). In the Silver Lake Playa, Mojave Desert, sand percentages showed peaks attributed to enhanced eolian activity between ca. 8,000 and 4,400 yr B2k (Kirby et al., 2015). Taken together, these data suggest a broad period between ca. 8,500 and 5,000 yr B2k of dry conditions in the Great Basin and eastern Sierra Nevada.

To provide a broader context for Holocene hydroclimate records and to investigate the spatial fingerprint of Middle Holocene aridity, we compiled an Aridity Index from 98 records—including those described above—of Holocene paleoclimate from the Pacific Southwest, Sierra Nevada, Great Basin, Southwest, and through

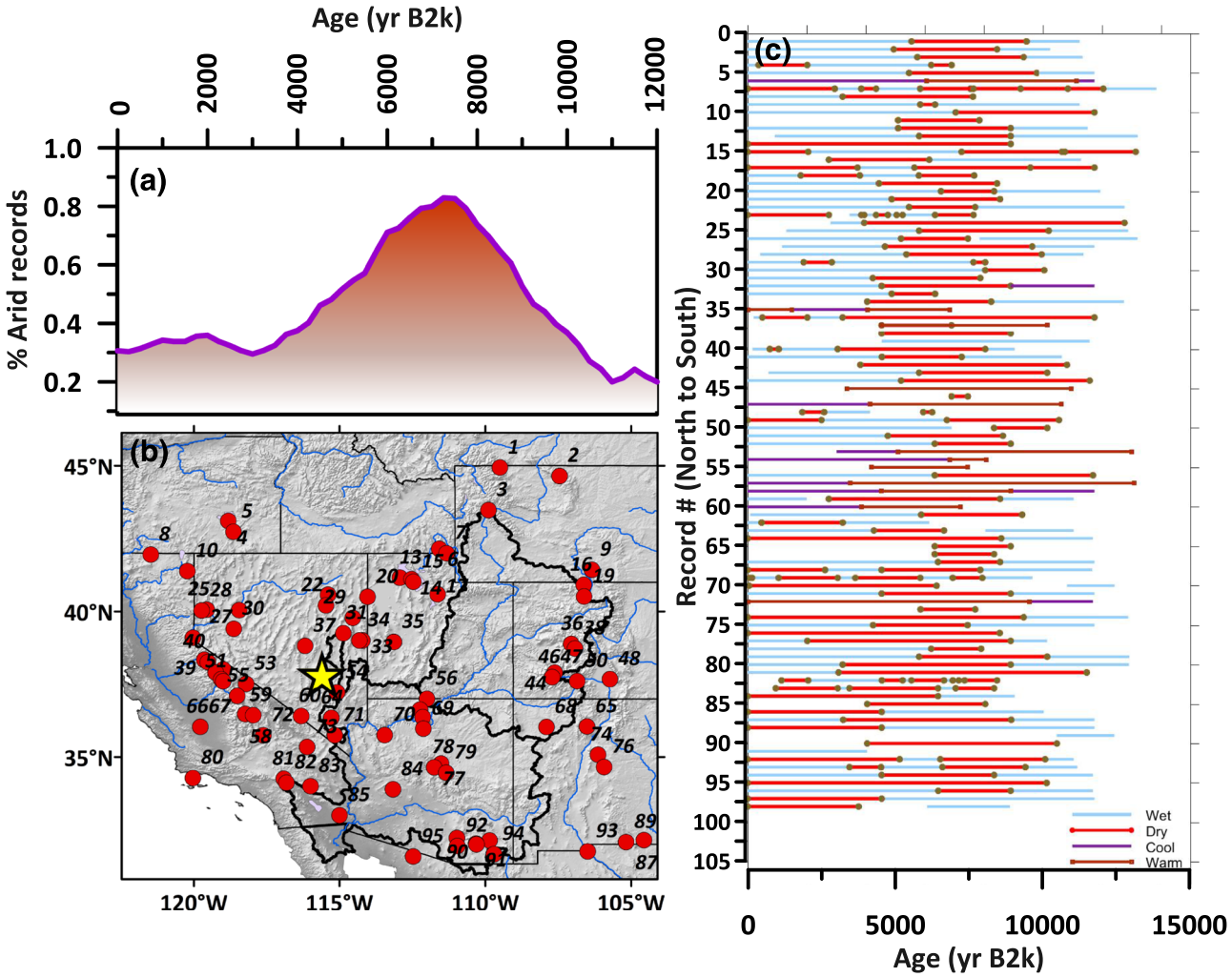

Figure 7. Aridity Index and site locations. (a) is the Aridity Index, showing a strong peak in sites recording their driest Holocene conditions between ca. 9,000 and 5,000 yr B2k. (b) shows location of records arranged by latitude and record number in Data set S3, which contains additional site details. Yellow star is Leviathan Cave, and black thick black outlines are the upper and lower Colorado River Basins. (c) shows all records coded into hydroclimate state, with red indicating aridity and light blue less aridity or wetter conditions.

the Rocky Mountains (Data Set S3, Figure 7). We included proxy records of effective moisture, such as lake sediment records and, when possible, included midden data, though we note that the latter are discontinuous, and the author's interpretations are often incomplete or contradictory. We assigned "wet," "dry," "cold," and "warm" states following the author's interpretation of climate conditions, with the authors' provided chronology, which in the publications were sometimes presented as generalized age ranges. Because many of these records were published without sufficient archived data, we did not attempt to complete new age modeling on their data and instead focus on the author's subjective interpretations of climate states in their stated time intervals. To increase the sample size and inclusiveness, we did not screen the records for chronological age density in order to provide the broadest possible summary of hydroclimate records. The provided ^{14}C ages were calibrated into calendar years before the year 2,000 (yr B2k) using IntCal13 with range of 95.4% and reporting the mean ± one σ ages, rounded to 10 yr; where no age uncertainty was provided, calibration input assumed uncertainty of ±100 ^{14}C yr. We did not tally fire/charcoal records, as the links to climatic change are not always clear. A running percentage of aridity records was tallied by summing arid records into 250 yr intervals to approximate the typical radiocarbon age uncertainty (Data Set S4). Because many of the records had sparse dating control, variable sample resolution, and many of the records did not have archived data, we

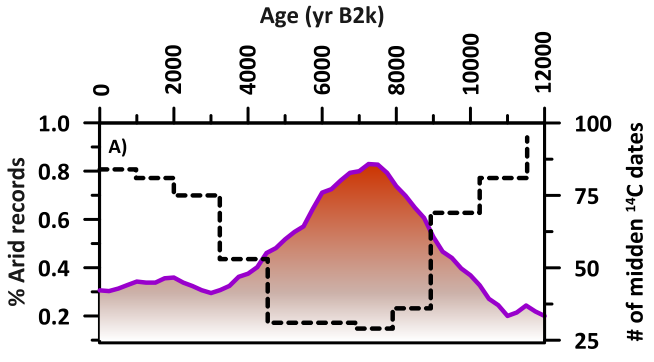

Figure 8. Correlation of the Southwest Aridity Index with a histogram of radiocarbon-dated middens. The clear minimum of dated middens (histogram recalibrated into yr B2k) from the early to middle Holocene coincides with peak aridity in the Southwest. While previously attributed to sampling bias by midden investigators, this comparison suggests that the dearth of middens dating to the middle Holocene may be partly due to arid conditions.

consider the aridity time series as a semi-quantitative index of aridity: The height of the curve in Figure 7 represents the number of records in which drought was evident. Further, because of the large sample size and conservative 250-yr age bins, age errors associated with individual records should not have a major effect on the final Aridity Index, particularly on the scale of the Early, Middle, and Late Holocene. The aridity data in many of the proxies, lake levels being a prime example, represent effective moisture that is precipitation minus evapotranspiration. Other proxies (like pollen) may record growing season precipitation more directly (Bartlein et al., 2014; Harrison et al., 2016). As such, the Aridity Index does not determine whether more-arid conditions are due to reduced precipitation or increased evapotranspiration or some combination of the two. We emphasize that it is possible to have periods of less effective moisture even during times of increased precipitation providing evapotranspiration exceeds the precipitation increase.

The Aridity Index time series demonstrates that regional climate during the Middle Holocene Aridity Intervals was mostly warmer and drier than the Late Holocene (Figure 7), and such arid conditions extended from the Pacific Southwest to the Sierra Nevada, Great Basin, Mojave Desert, Colorado River Basin, and Rocky Mountains (Anderson, 2012; Kirby et al., 2013; MacDonald et al., 2016; Shuman & Serravezza, 2017). The greatest number of records indicate that dry conditions peaked at around 7,400 yr B2k, lagging behind the ~10,000 to 11,000 yr B2k peak in summer insolation. The widespread aridity is supported by observation of correlated modern climates from the Mojave, Great Basin, and Colorado River basin regions in Figure 2. Some summer rainfall sensitive biotic proxy records indicate stronger Middle Holocene summer rainfall than today, consistent with observations and climate dynamical modeling that suggests an increase in the strength of the North American monsoon (Harrison et al., 2003; Metcalfe et al., 2015; Thompson et al., 1993). A stronger summer monsoon during the Middle Holocene is supported by a diverse array of evidence but could still be registered as increased aridity at many sites if potential evapotranspiration due to warmer conditions exceeded the increase in precipitation. However, the high Aridity Index values in the Middle Holocene indicate greatest aridity at most sites, a climatic feature that is particularly evident in the low lake levels recorded across the Great Basin, Mojave Desert, and southern Rocky Mountains. As such, the sites showing aridity during the Middle Holocene indicate that summer wetting due to a stronger monsoon was not strong enough to counteract the effects of higher temperatures or winter drying at multi-annual time scales, likely because of reduced effective infiltration during the summer. This contention is supported for the Great Basin, where modern data show that summer moisture is ineffective in recharging aquifers (Winograd et al., 1998), a finding consistent with our observation in stalagmite LC-1 of reduced growth rates and high $\delta^{13}C$ values prior to the Middle Holocene.

We also show a biotic response to the arid climates of the Middle Holocene in Figure 8. We compare a histogram of radiocarbon-dated packrat middens (with bin limits calibrated to calendar years B2k) in the Southwest (Webb & Betancourt, 1990) to the Aridity Index, and the two are inversely correlated. While the lack of Middle Holocene middens had been previously attributed to the investigator's sampling bias, we show that a plausible alternative is widespread aridity, potentially resulting in fewer middens through a reduction in packrat population sizes and/or decreased preservation potential. The potential for Middle Holocene aridity to have driven changes in species composition and richness is also supported by the data from Homestead Cave, Nevada, which showed a decline in small mammal species and diversity due to extreme aridity (Grayson, 2000).

3.5. Potential Forcings on Great Basin Paleoclimate

We previously documented the strong correlation between Great Basin paleoclimate and Milankovitch forcing on precessional time scales over the last 175,000 yr from Leviathan (LC-1), Pinnacle (Lachniet, 2016; Lachniet et al., 2014, 2017), and Lehman Caves (Shakun et al., 2011), Nevada (Figure 1). We observed that Great Basin $\delta^{18}O$ showed a strong similarity to 65°N summer insolation (21 June to 21 August), but lagged behind it by >3,000 yr, a difference in timing we linked to indirect forcing by the Earth's cryosphere. The

climatic evolution since the Younger Dryas also supports this overall orbital forcing of Holocene paleoclimate in the Great Basin. For example, summer insolation (21 June to 21 August) peaked at ca. 11,000 to 10,000 yr B2k, while peak warmth (as inferred from the LC-1 stalagmite record) in the Great Basin was ca. 8,400 yr B2k. The peak in the Aridity Index at ca. 7,400 yr B2k also lagged the summer insolation peak by about three millennia. Then, the Great Basin gradually returned to cooler conditions between ca. 8,400 and 4,100 yr B2k. A decrease in Leviathan Cave $\delta^{18}O$ coincides with decreasing summer insolation, and this trend to apparently cooler conditions (or more high-latitude moisture) was also associated with an increase in soil productivity and growth rate, which we attribute to an increase in effective moisture. The trend to a cooler and wetter climate over the Middle to Late Holocene is consistent with the precessional scale forcing of Great Basin paleoclimate also observed over the last 175,000 yr (Figure 1).

But what were the mechanisms of sub-orbital-scale paleoclimatic change that may explain the structure and timing of Holocene climate events? General circulation model (GCM) studies have attempted to place Holocene paleoclimate records in the broader context of orbital, ice-sheet, and atmospheric forcings (Bartlein et al., 2014; Harrison et al., 2016; Renssen et al., 2005; Zhang et al., 2010). During deglaciation, both a retreat of the Laurentide Ice Sheet and rising summer insolation may have contributed to regional warming (Renssen et al., 2012), and greatest insolation seasonality was reached during the Early Holocene at ~10,000 yr B2k. Greenhouse gas concentrations (CO_2 and CH_4) reached near pre-Industrial levels by ca. 11,000 yr B2k, and the Laurentide Ice Sheet was almost completely gone by ca. 7,000 yr B2k. In contrast to these forcings, the LC-1 $\delta^{18}O$ record showed peak warming at 8,400 yr B2k, with a cooling toward the modern that is not consistent with ice sheet retreat and greenhouse gases but is similar to the decreases in both northern hemisphere summer insolation and insolation seasonality. This observation indicates that the evolution of Great Basin paleoclimate is more strongly tied to insolation than other potential forcings (Lachniet et al., 2017), as is clearly evident in Figure 1.

Some studies suggested that long-term insolation changes influenced Arctic sea ice via cooling from the Middle to Late Holocene (Lachniet et al., 2017; Renssen et al., 2005; Zhang et al., 2010), in association with positive ice-albedo and ice-insulation feedbacks (Yoshimori & Suzuki, 2019). Proxy evidence for decreasing Arctic summer warmth over the Middle to Late Holocene is also shown by the decrease in prevalence of melt layers in the Agassiz cap (Fisher et al., 1995) from a maximum at ca. 9,100 yr B2k to a near-modern minimum levels at about 4,400 yr B2k, similar in timing to the aridity intervals in our speleothem data and to the Aridity Index. Widespread midlatitude drying during the Middle Holocene, consistent with our analysis, has been attributed to orbitally induced feedback responses originating in the Arctic that resulted in changes in the latitudinal temperature gradient (Routson et al., 2019). Paleoclimatic change in the Great Basin is consistent with the hypothesis that the region responded to summer insolation and feedbacks involving the Arctic and/or the cryosphere that amplified high-latitude warming and increased the latitudinal temperature gradient (Cohen et al., 2020; Routson et al., 2019). We extend this observation with our new Aridity and sea ice indices to show that the timing of Middle Holocene dry winter conditions in the Southwest coincided with a warmer Arctic, reduced sea ice extent, and that these changes lagged the peak in summer insolation by several millennia. The lag time in warmth, aridity, and low sea ice extents relative to orbital forcing suggests that higher summer insolation could have contributed to these parameters in the Middle Holocene but was unlikely to be the primary forcing.

Another possible cause of Holocene Great Basin paleoclimatic change involves variation in the strength and frequency of the El Niño/Southern Oscillation (ENSO) (Metcalfe et al., 2015) or, more broadly, the temperature evolution of the Pacific Ocean (Linsley et al., 2010). The transition to wet Late Holocene conditions in the Great Basin may have been driven by enhanced strength and/or variability of ENSO, particularly in the warm (El Niño) phase (Barron & Anderson, 2011), which has been linked through modeling studies to decreasing summer insolation over the Holocene (Cane & Clement, 1999). Arid conditions in the Sierra Nevada and Mojave Desert of the western United States during the Middle Holocene were interpreted to be related to La Niña-like conditions in the tropical Pacific Ocean (Kirby et al., 2015; MacDonald et al., 2016), an ocean-atmosphere linkage that today is associated with drought conditions.

To test among these ideas, we completed a Monte Carlo-based least-squares regression analysis. Ocean and terrestrial paleoclimate time series were interpolated to a common interval (from most recent shared ages to 11,700 yr B2k) using a 250-yr time step and filtered using a 300-yr moving average. Correlations were

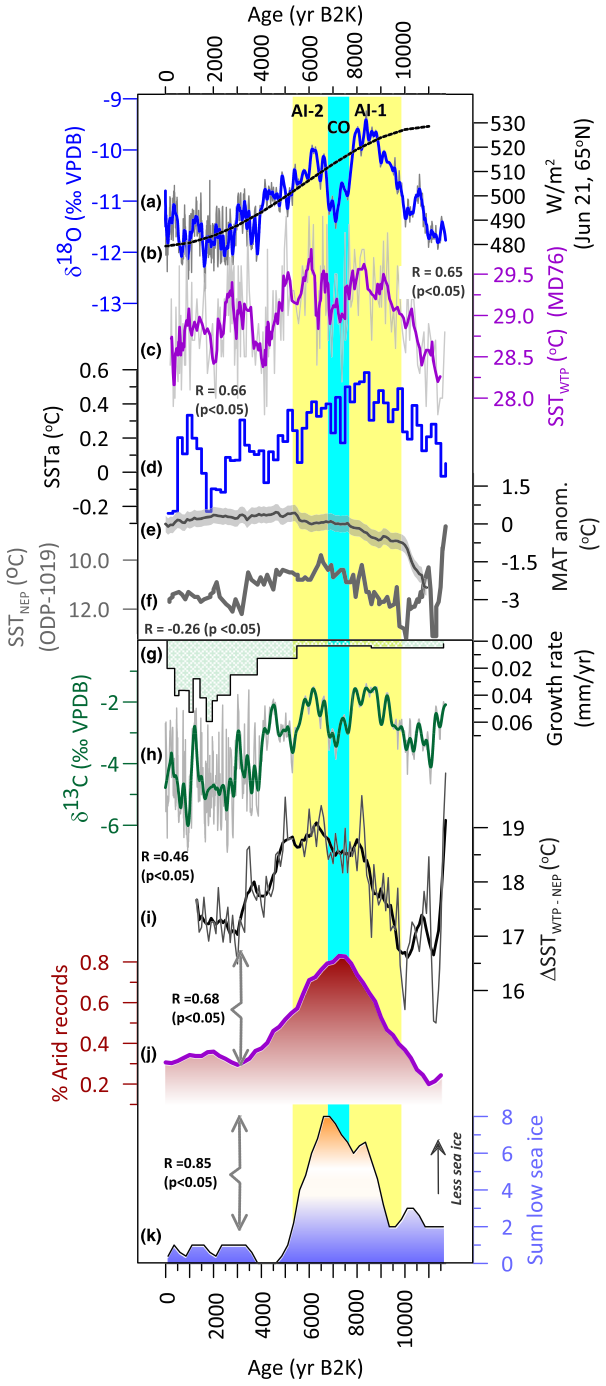

Figure 9. Great Basin paleoclimate driven by sea surface temperature. (a) Leviathan LC-1 speleothem $\delta^{18}O_{ivc}$ (this study); (b) 21 June insolation at 65°N; (c) western tropical Pacific SST (MD76, Stott et al., 2004); (d) compilation of WTP SST anomalies (Linsley et al., 2010); (e) pollen-based mean annual air temperature anomalies for North America and Europe (Marsicek et al., 2018); (f) Northeastern Pacific SST (ODP-1019, Barron et al., 2003); (g) LC-1 growth rate on inverted scale (this study); (h) LC-1 $\delta^{13}C$ values (this study); (i) SST gradient between the Western tropical (MD76) and Northeastern Pacific (ODP1019); (j) Aridity Index showing percentage of records of extreme aridity (this study); (k) sum of low sea ice proxies in the Arctic indicating lowest sea ice extent in the middle Holocene, from Stranne et al. (2014).

determined using least-squares regression on both the interpolated and filtered data. For significance testing of the correlations on the filtered data, Monte Carlo significance testing was used to create 10,000 random time series with the same autocorrelation structure as the input time series, and each resulting time series was correlated to the predictor time series to generate a population of Pearson *R* values from which quantiles were determined to assess the significance level of the observed correlations. The filtered time series in general better show the broad-scale climate teleconnections because much of the high-frequency variability is removed. In the text, we indicate whether the correlations were based on the paired filtered or unfiltered data, and we present those correlations that passed Monte Carlo significance testing.

To test for a similarity with the evolution of Pacific Ocean sea surface temperature, we correlated the Leviathan data and the Aridity Index to SST records from the western tropical Pacific (WTP) cores MD76 and MD81 (Stott et al., 2004), Northeastern Pacific Ocean (NEP; site ODP-1019), and with the Gulf of Mexico (MD02–2575) (Barron et al., 2003; Ziegler et al., 2008). Further, to emphasize the broad Holocene trends in SST evolution, we compared our data to a compilation of SST anomalies (SSTa) from eight cores in the western tropical Pacific warm pool (Linsley et al., 2010). A strong predictor of Leviathan $\delta^{18}O_{ivc}$ is SST in the western tropical Pacific, which captures the cool-warm-cool changes over the Holocene (filtered $\delta^{18}O_{ivc}$ vs. MD76 SST, $r = 0.65$, $p < .05$), and even the cool oscillation centered on 7,000 yr B2k in the stalagmite has a counterpart SST decrease in core MD76 (Figure 9). More strikingly, the correlation between Leviathan and the compilation of WTP SST anomalies (Linsley et al., 2010) is also high (unfiltered $\delta^{18}O_{ivc}$ vs. WTP SSTa = 0.66, $p < .05$; Figure 9). Gulf of Mexico SST is similarly correlated to the Leviathan Holocene record (filtered $\delta^{18}O_{ivc}$ vs MD2575 SST, $r = 0.73$, $p < .05$, not shown in Figure 8): Both records share a gradual deglacial warming, peak warmth during the Middle Holocene, then cooling in the Late Holocene. An insignificant inverse correlation to $\delta^{18}O_{ivc}$ is observed for the proximal northeast Pacific (ODP-1019).

We also show that Leviathan Cave and Southwestern aridity are linked to the spatial structure of Pacific Ocean SST (Figure 9) over the Holocene, in a similar manner as today. The moisture-sensitive Leviathan $\delta^{13}C$ record is positively correlated to the WTP SST at site MD81 (unfiltered $\delta^{13}C$ vs. MD81, $r = 0.45$, $p < .05$), to the WTP SSTa (unfiltered $\delta^{13}C$ vs. SSTa, $r = 0.50$, $p < .05$), and to the SST gradient between the western tropical and northeastern Pacific (unfiltered $\delta^{13}C$ vs. $\Delta SST_{WTP\text{-}NEP}$, $r = 0.40$, $p < .05$). An outlier is the slight decrease in stalagmite $\delta^{18}O_{ivc}$ and $\delta^{13}C$ values during the cool oscillation, which do not have a counterpart in the Aridity Index which instead showed the greatest number of dry records. We do not have a good explanation for this observation, but it may relate to the higher resolution and strong chronological control of the U-series dated stalagmite compared to the 250-yr bin size and significantly lower-resolution radiocarbon dating of the records comprising the Aridity Index. We chose the MD76 and ODP1019 sites to construct the cross-Pacific ΔSST record because the Western tropical Pacific is warm during La Niña events, and the site-proximal northeast Pacific Ocean is cool, and the combination of the two should be a proxy for the strength of the ocean regions affecting aridity in the Southwest. The $\Delta SST_{WTP\text{-}NEP}$ gradient shows that when zonal SST gradients are large, similar to a La Niña structure, the Aridity Index is high (>70% of records show aridity; unfiltered Aridity Index vs. ΔSST_{WTP}-ETP, $r = 0.68$, $p < .05$; Figure 9). This correspondence of tropical Pacific spatial structure has been previously observed for Leviathan Cave and the Mojave Desert (Kirby et al., 2015), and we now show that it applies more broadly to the Southwest.

These relationships suggest a common origin. When tropical insolation is high, enhanced warming in the western tropical Pacific increases the WTP to ENP SST gradient, a configuration in the modern climate that is also associated with aridity in the west (Clement et al., 2000; Liu et al., 2003). Following the pronounced arid intervals of the Middle Holocene, Late Holocene wetting commenced around 4,200 yr B2k when the Pacific zonal SST gradient weakened, as seen in decreasing $\delta^{13}C$, faster growth rates, a cooler WTP, and fewer extremely arid records (<40%).

In contrast, the time evolution of aridity and warmth (high speleothem $\delta^{18}O$ values) does not coincide with pollen-inferred regional temperature change over North America and Europe (Marsicek et al., 2018). While Southwestern aridity peaked ~8,400 yr B2k in the Leviathan record, and ~7,400 yr B2k in the Aridity Index, pollen-based temperature reconstructions suggested warmest conditions were reached after ~5,000 yr B2k when the Aridity Index had already begun to transition to wetter neopluvial conditions (Figure 9). The lack of coherence between the pollen-based temperatures and hydroclimate in the Southwest suggests that a

direct temperature control was less important to aridity than atmospheric circulation and/or teleconnections or that the speleothem and pollen data are recording different seasons or processes.

Highest $\delta^{18}O$ values, slow growth rates, and high $\delta^{13}C$ values in stalagmite LC-1 indicate warm and arid conditions during the Middle Holocene. The timing of Great Basin paleoclimate changes is coincident with reduced Arctic sea-ice extent associated with the orbitally controlled Holocene thermal maximum (Funder et al., 2011; Kaufman et al., 2004). The relationship between high Arctic temperatures and low sea ice is consistent with the hypothesis of a teleconnection to the Southwest in a manner analogous to today, where a warm Arctic and low sea ice have been linked to dry conditions (Swain et al., 2017). To test this idea in more detail, we created a summed distribution of low Arctic sea ice proxies from data reviewed by Stranne et al. (2014) (their Figure 4) with ages calibrated into years B2k. These records comprise paleo-proxy data on Arctic sea ice and include abundance of drift wood on Arctic beaches, beach ridges, and geochemistry of sediment cores, for example, the IP_{25} proxy (Stranne et al., 2014). The records are concentrated in the North Atlantic Ocean sector of the Arctic and come from the central Arctic Ocean (Cronin et al., 2010; Hanslik et al., 2010), off the Chukchi Sea (De Vernal et al., 2005), Ellesmere Island (England et al., 2008), North and Central Greenland (Bennike, 2004; Funder et al., 2011), the Canadian Arctic archipelago (Belt et al., 2010; Dyke et al., 1996; Vare et al., 2009), and west of Spitsbergen and the East Greenland Shelf (Müller et al., 2012). We digitized the start and end times of the intervals represented by low sea ice and summed the number of sites recording low sea ice into 250-yr intervals. The summed low sea ice index thus indicates the number of sites around the Arctic (primarily in the Atlantic sector) that indicate low sea ice conditions at a given time. As with our approach for the Aridity Index, we used the low sea ice proxy data on the original author's chronology and interpretation. We also note that the first strong evidence of significantly reduced sea ice in the Arctic only occurred following deglacial warming in the Early to Middle Holocene, when other evidence indicates warm Arctic conditions (e.g., melt events in the Agassiz Ice Cap, Fisher et al., 1995), so older sea ice records are not present in the sea ice compilation because of unfavorable conditions for its growth. There is a strong similarity in timing of Southwest aridity and Arctic sea ice—at least for the variations captured by the (Stranne et al., 2014) study—and the two indices are strongly correlated (Figure 9); unfiltered aridity index versus low sea-ice records, $r = 0.85$, $p < .05$). Both the aridity and low sea ice data show peak warm conditions on a sub-orbital scale between ~9,000 and 5,000 yr B2k, which coincided with widespread Arctic warmth between 8,950 ± 2,100 and 5,950 ± 2,600 yr B2k (Briner et al., 2016; Kaufman et al., 2004). Both the aridity and low sea ice data are lagged for a few millennia after the peak in summer insolation, similar to what we observe in the Leviathan Cave isotopic data. Low Middle Holocene sea ice extent has been attributed to increased Northern Hemisphere summer insolation (Renssen et al., 2005; Zhang et al., 2010), and sea ice may have disappeared completely during summers (Stranne et al., 2014) coincident with the Middle Holocene arid intervals.

4. Discussion

Our comparisons show that the evolution of Holocene climate in the Great Basin and other areas of the Southwest coincided with climatic change in other regions. For example, our $\delta^{18}O_{ivc}$ record shows strong correlations to SST in the western tropical Pacific Ocean and to the SST gradient across the tropical Pacific Ocean (Figure 9). These observations suggest that the Pacific Ocean's influences on aridity during the Holocene were similar to those observed today. Importantly, the precessional-scale $\delta^{18}O_{ivc}$ signal—including the peak warmth around 8,400 yr B2k and cooling to the modern—cannot be explained by a simple hypothesis of ice sheet forcing, because the North American ice sheets had largely disappeared prior to ~7,000 yr B2k while the Great Basin shows a cooling trend along with decreasing insolation. If ice sheet retreat were the primary control on Great Basin $\delta^{18}O$ variations, we would expect to see constant values following deglaciation. Instead, we observe a $\delta^{18}O$ decrease that is similar in magnitude but in the opposite direction, to the $\delta^{18}O$ increase coming out of the Younger Dryas.

Additionally, we consider the potential linkages between Middle Holocene aridity in the Southwest and the extended period of warm and low sea-ice conditions in the Arctic between ca. 9,000 and 5,000 yr B2k (Briner et al., 2016; Kaufman et al., 2004; Stranne et al., 2014). Does sea-ice loss in the Arctic force atmospheric circulation change in the Southwest? Or do the two regions respond more simply to a common forcing without middle- to high-latitude interactions? Some evidence suggests that atmospheric circulation responds to

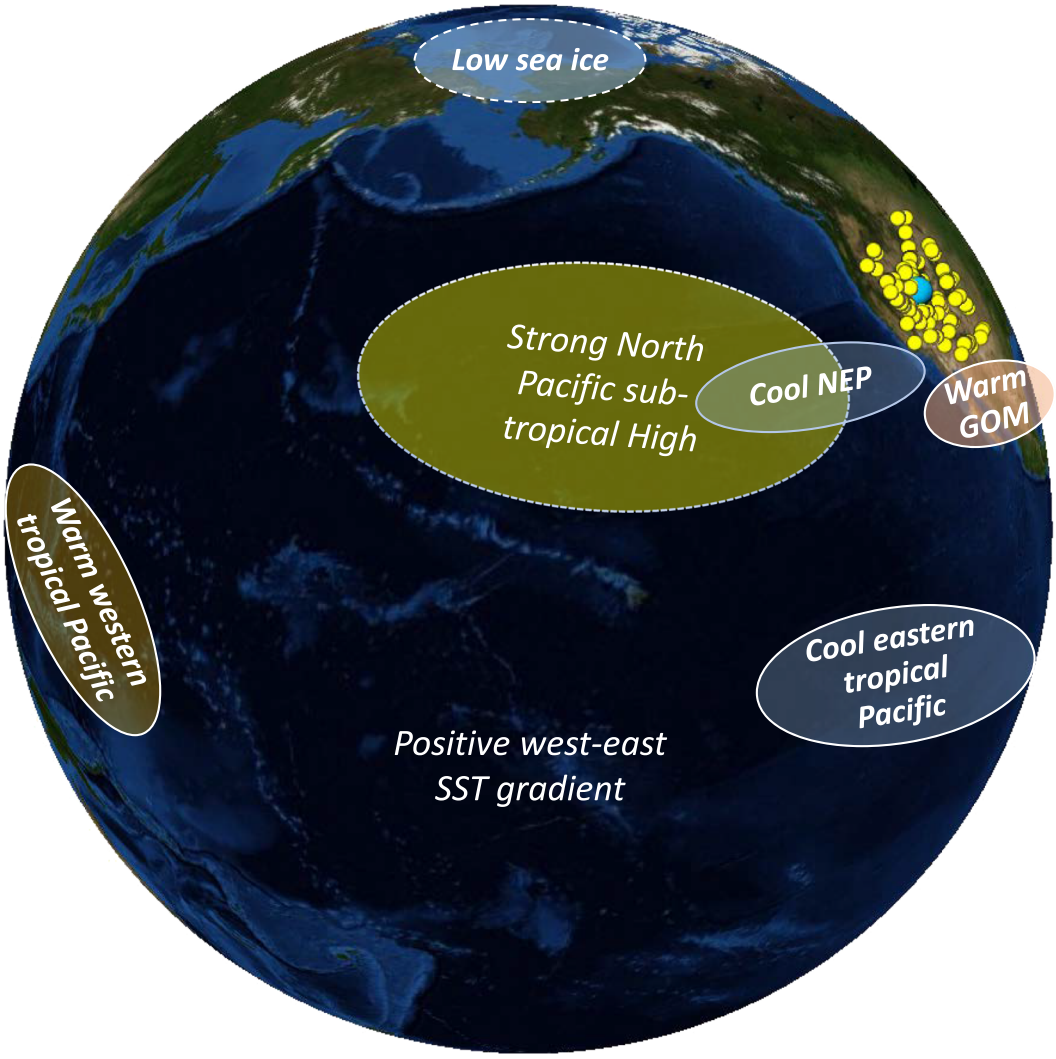

Figure 10. Climate states contributing to aridity in the western United States. The widespread spatial pattern of heat and aridity in the Western United States was associated with a warm GOM, cool NEP, and a large west-to-east tropical Pacific SST gradient, producing high pressure and aridity over the Southwest. Yellow dots are sites compiled in the Aridity Index, and the large blue dot is Leviathan Cave, Nevada. See SM for site details.

climatic anomalies in the Arctic, but the strength, persistence, and causality of linkages between these regions remain a point of debate in the literature (Cohen et al., 2020; Overland et al., 2016). For example, observational evidence suggests that winter atmospheric circulation responds strongly to summer sea-ice cover (Francis et al., 2009) and that summer warming may persist into the autumn and winter (Park et al., 2019). However, the potential connections between Arctic amplification and midlatitude weather are not yet considered robust for the modern period because of the short instrumental record and may be instead related instead to natural variability (Cohen et al., 2020). For a longer time-scale perspective on these potential linkages, indications from the paleoclimate record and model-data comparisons are useful.

An analysis of proxy data and model output has shown that the combination of higher summer insolation during the Middle Holocene resulted in Arctic amplification of hemispheric temperature anomalies, a decrease in the latitudinal temperature gradient, and a general drying of the midlatitudes (Routson et al., 2019). These linkages operate in a manner consistent with our observations of high speleothem $\delta^{18}O_{ivc}$ values and aridity during the Middle Holocene when the Arctic was warm and sea ice was low. Other model results indicate that summer insolation can control both winter sea-ice extent and winter

temperature, providing a plausible link between the Arctic and Great Basin climates (Renssen et al., 2005). Warmer winter temperatures may have also resulted from decreased summer sea ice cover via the ice insulation/temperature feedback, with less sea ice cover facilitating ocean to atmosphere heat exchange. While the modeling and observational data for the instrumental period suggest ambiguity in exactly how, or if, Arctic feedbacks influence midlatitude climate (Cohen et al., 2020), the paleoclimatic data suggest similarities between the two in the Middle Holocene (Routson et al., 2019).

Increased summer insolation in the northern hemisphere likely was the ultimate driver of both the changes in the Arctic and warming of the western tropical Pacific Ocean, and those changes may have provoked enhanced aridity in the West in a manner analogous to the modern climate, with a strengthened subtropical high pressure cell and a reduced latitudinal temperature gradient (Routson et al., 2019). There is some evidence that the Middle Holocene is not a strict analog for future climate changes (Bartlein et al., 2011; Renssen et al., 2012), whereas other work found that both insolation and greenhouse gas increases can result in Arctic warming (Yoshimori & Suzuki, 2019). Future high-latitude warming and sea ice loss, whether from higher northern hemisphere insolation as described here or from increasing greenhouse gases, may be of similar magnitude as during the Middle Holocene (Schmidt et al., 2014).

Additionally, our documentation of extreme millennial-length Holocene aridity has important implications for Southwestern hydroclimate and its potential links to the Arctic and Pacific regions (Figure 10). First, our speleothem data and the Aridity Index show that the Southwest experienced arid intervals prior to anthropogenic influence that were hotter, mostly drier, and longer than any other droughts over the last four millennia, including the so-called megadroughts and "worst-case" twelfth century Colorado River drought (Cook et al., 2010; Woodhouse et al., 2010). This observation is important because it suggests that such aridity might return in the future if boundary conditions in the Pacific Ocean and/or the Arctic return to Middle Holocene-like states. Second, our data are consistent with and affirm on Holocene timescales the conclusion of a strong Pacific Ocean control on modern western North America hydroclimate (Anderson, 2012; Kirby et al., 2013; Kirby et al., 2015; MacDonald et al., 2016; Shuman & Serravezza, 2017), with a warming WTP associated with western heat and aridity due to strengthening of the subtropical ridge and northward displacement of storm tracks (Hermann et al., 2018; Sewall, 2005; Swain et al., 2017). The equatorial Pacific atmosphere is projected to warm in the future (Kay et al., 2014), and such warming may initiate more persistent atmospheric ridging off the West Coast of North America. While the future response of ENSO to greenhouse warming is not entirely clear (Collins et al., 2010), should a trend to more La Niña events occur it would amplify aridity in the Southwest (Koutavas & Joanides, 2012; Stott et al., 2004) and weaken aridification for more El Niño events (Cai et al., 2018). Even absent ENSO variability, increased evaporative demand and decreased snow to sustain Colorado River flow is projected for a warming world (Seager & Vecchi, 2010; Woodhouse et al., 2016). Third, because the tropical and midlatitude North Atlantic is already warming and will continue to do so in coming centuries (Cheng et al., 2017; Kirtman et al., 2013; Polyakov et al., 2010), the Southwest is also likely to warm and dry if past associations continue for the future. Fourth, the strong correlation between aridity, Arctic warmth, and low Arctic sea ice extents has potential future implications: Should the hypothesis put forward by Francis et al. (2009) that sea ice influences midlatitude temperatures turn out to be a robust feature of the climate system, reduced sea ice extent may lead to a reduced latitudinal temperature gradient resulting in weaker midlatitude westerly flow and weaker cyclonic conditions (Routson et al., 2019) and a strengthening of the subtropical high pressure cell (Wang et al., 2014), resulting in warmer and drier conditions in the Southwest (Cvijanovic et al., 2017; Francis et al., 2009; Renssen et al., 2005; Sewall, 2005; Swain et al., 2017) (Figure 10).

Given this long-term robust coupled variability between Southwestern aridity to tropical Pacific temperatures and conditions in the Arctic, we posit that Southwest is at risk of a long-term aridification to extremes that exceed in severity the limits of Late Holocene hydroclimate variations evident from the tree-ring record. Should the causality of the teleconnections be affirmed, then further climatic changes in the tropical Pacific and Arctic are likely to impact Southwestern hydroclimate via atmospheric teleconnections that act reduce winter precipitation (Routson et al., 2019), having potentially profound implications for sustaining human populations reliant on winter snowpack for water resources in the Colorado and Grande River Basins. The true worst-case dry interval in the Southwest may, in reality, be more analogous to the millennial-length Middle Holocene aridification than to the relatively minor so-called megadroughts of

the Medieval. If true, future aridity is likely to be of longer duration (Seager & Vecchi, 2010; Woodhouse et al., 2016) than historical droughts impacting water supply in the Southwest (Cook et al., 2015; Udall & Overpeck, 2017). A case in point is the projection that Colorado River flow may be reduced by up to 50% by the year 2100 under high greenhouse gas emissions scenarios due to lower snowpack and increased evaporation (Udall & Overpeck, 2017) and the possibility of a 60% reduction of snowfall in the Colorado Basin headwaters (Fyfe et al., 2017). Because future climate outcomes are contingent on decisions made today, adoption of targets to reduce greenhouse gas emissions to minimize oceanic and Arctic warming is insurance to mitigate future Southwestern aridification. "Business as usual" scenarios for anthropogenic warming carry the risk of tipping the Southwest into a state of extended aridification.

Data Availability Statement

Stalagmite LC-1, the Southwest Aridity Index, and precipitation $\delta^{18}O$ data are available on the NOAA Paleoclimatology database (https://www.ncdc.noaa.gov/paleo/study/29592). Correspondence and requests for materials should be addressed to Matthew S. Lachniet (matthew.lachniet@unlv.edu).

Acknowledgments
We thank the Ely District of the Bureau of Land Management for cave access and collection permits and the Southern Nevada Grotto for field support. This study was supported by NSF grant AGS-1405546 to UNLV and 1405557 to UNM and facilities grants EAR-0521196 to UNLV and EAR-0326902 to UNM. We thank the anonymous reviewers for their insightful and thorough comments of this manuscript.

References

Adams, K. D., & Rhodes, E. J. (2019). Late Pleistocene to present lake-level fluctuations at pyramid and Winnemucca lakes, Nevada, USA. *Quaternary Research*, *92*(1), 146–164. https://doi.org/10.1017/qua.2018.134

Alley, R. B., & Agustsdottir, A. M. (2005). The 8k event: Cause and consequences of a major Holocene abrupt climate change. *Quaternary Science Reviews*, *24*(10-11), 1123–1149. https://doi.org/10.1016/j.quascirev.2004.12.004

Amundson, R. G., Chadwick, O. A., Sowers, J. M., & Doner, H. E. (1988). Relationship between climate and vegetation and the stable carbon isotope chemistry of soils in the eastern Mojave Desert, Nevada. *Quaternary Research (New York)*, *29*(3), 245–254. https://doi.org/10.1016/0033-5894(88)90033-6

Anderson, L. (2012). Rocky Mountain hydroclimate: Holocene variability and the role of insolation, ENSO, and the north American monsoon. *Global and Planetary Change*, *92-93*, 198–208. https://doi.org/10.1016/j.gloplacha.2012.05.012

Anderson, R. S. (1990). Holocene Forest development and Paleoclimates within the central sierra-Nevada, California. *Journal of Ecology*, *78*(2), 470–489. https://doi.org/10.2307/2261125

Anderson, R. S., & Smith, S. J. (1994). Paleoclimatic interpretations of meadow sediment and pollen stratigraphies from California. *Geology*, *22*(8), 723–726. https://doi.org/10.1130/0091-7613(1994)022<0723:piomsa>2.3.co;2

Ault, T. R., Mankin, J. S., Cook, B. I., & Smerdon, J. E. (2016). Relative impacts of mitigation, temperature, and precipitation on 21st-century megadrought risk in the American southwest. *Science Advances*, *2*(10). https://doi.org/10.1126/sciadv.1600873

Aziz, O. A., Tootle, G. A., Gray, S. T., & Piechota, T. C. (2010). Identification of Pacific Ocean Sea surface temperature influences of upper Colorado River basin snowpack. *Water Resources Research*, *46*, W07536. https://doi.org/10.1029/2009WR008053

Bacon, S. N., Burke, R. M., Pezzopane, S. K., & Jayko, A. S. (2006). Last glacial maximum and Holocene lake levels of Owens Lake, eastern California, USA. *Quaternary Science Reviews*, *25*(11-12), 1264–1282. https://doi.org/10.1016/j.quascirev.2005.10.014

Barron, J. A., & Anderson, L. (2011). Enhanced Late Holocene ENSO/PDO expression along the margins of the eastern North Pacific. *Quaternary International*, *235*, 3–12. https://doi.org/10.1016/j.quaint.2010.02.026

Barron, J. A., Heusser, L., Herbert, T., & Lyle, M. (2003). High-resolution climatic evolution of coastal northern California during the past 16,000 years. *Paleoceanography*, *18*(1), 1020. https://doi.org/10.1029/2002PA000768

Bartlein, P. J., Harrison, S. P., Brewer, S., Connor, S., Davis, B. A. S., Gajewski, K., et al. (2011). Pollen-based continental climate reconstructions at 6 and 21 ka: A global synthesis. *Climate Dynamics*, *37*(3), 775–802. https://doi.org/10.1007/s00382-010-0904-1

Bartlein, P. J., Hostetler, S. W., & Alder, J. R. (2014). Paleoclimate. In G. Ohring (Ed.), *Climate Change in North America* (pp. 1–52). Cham, Switzerland: Springer.

Belt, S. T., Vare, L. L., Massé, G., Manners, H. R., Price, J. C., Maclachlan, S. E., et al. (2010). Striking similarities in temporal changes to spring sea ice occurrence across the central. *Canadian Arctic Archipelago over the last 7000 years*, *29*(25–26), 3489–3504. https://doi.org/10.1016/j.quascirev.2010.06.041

Bennike, O. (2004). Holocene Sea-ice variations in. *Greenland: onshore evidence*, *14*(4), 607–613. https://doi.org/10.1191/0959683604hl722rr

Benson, L., Burdett, J., Lund, S., Kashgarian, M., & Mensing, S. (1997). Nearly synchronous climate change in the northern hemisphere during the last glacial termination. *Nature*, *388*(6639), 263–265. https://doi.org/10.1038/40838

Bischoff, J. L., Stafford, T. W. Jr., & Rubin, M. (1997). A time-depth scale for Owens Lake sediments of core OL-92: Radiocarbon dates and constant mass-accumulation rate. In *An 800,000-Year Paleoclimatic record from core OL-92, Owens Lake, Southeast California*, (Vol. special paper 317, pp. 91–98). Boulder, Colorado: Geological Society of America.

Blinn, D. W., Hevly, R. H., & Davis, O. K. (1994). Continuous Holocene record of diatom stratigraphy, paleohydrology, and anthropogenic activity in a spring-mound in southwestern United States. *Quaternary Research*, *42*(2), 197–205. https://doi.org/10.1006/qres.1994.1069

Briner, J. P., McKay, N. P., Axford, Y., Bennike, O., Bradley, R. S., de Vernal, A., et al. (2016). Holocene climate change in Arctic Canada and Greenland. *Quaternary Science Reviews*, *147*, 340–364. https://doi.org/10.1016/j.quascirev.2016.02.010

Cai, W., Wang, G., Dewitte, B., Wu, L., Santoso, A., Takahashi, K., et al. (2018). Increased variability of eastern Pacific El Niño under greenhouse warming. *Nature*, *564*(7735), 201–206. https://doi.org/10.1038/s41586-018-0776-9

Cane, M., & Clement, A. C. (1999). A role for the tropical Pacific coupled ocean-atmosphere system on Milankovitch and millennial timescales; part II, global impacts. *Geophysical Monograph*, *112*, 373–383. https://doi.org/10.1029/gm112p0373

Cayan, D. R., & Roads, J. O. (1984). Local relationships between United States west coast precipitation and monthly mean circulation parameters. *Monthly Weather Review*, *112*(6), 1276–1282. https://doi.org/10.1175/1520-0493(1984)112<1276:LRBUSW>2.0.CO;2

Cheng, L., Trenberth, K. E., Fasullo, J., Boyer, T., Abraham, J., & Zhu, J. (2017). Improved estimates of ocean heat content from 1960 to 2015. *Science Advances*, *3*(3). https://doi.org/10.1126/sciadv.1601545

Clement, A. C., Seager, R., & Cane, M. A. (2000). Suppression of El Niño during the mid-Holocene by changes in the Earth's orbit. *Paleoceanography*, *15*(6), 731–737. https://doi.org/10.1029/1999PA000466
Coats, S., Smerdon, J. E., Cook, B. I., Seager, R., Cook, E. R., & Anchukaitis, K. J. (2016). Internal Ocean-atmosphere variability drives megadroughts in Western North America. *Geophysical Research Letters*, *43*, 9886–9894. https://doi.org/10.1002/2016GL070105
Cohen, J., Zhang, X., Francis, J., Jung, T., Kwok, R., Overland, J., et al. (2020). Divergent consensuses on Arctic amplification influence on midlatitude severe winter weather. *Nature Climate Change*, *10*(1), 20–29. https://doi.org/10.1038/s41558-019-0662-y
Collins, M., An, S.-I., Cai, W., Ganachaud, A., Guilyardi, E., Jin, F.-F., et al. (2010). The impact of global warming on the tropical Pacific Ocean and El Nino. *Nature Geoscience*, *3*(6), 391–397. https://doi.org/10.1038/ngeo868
Cook, B. I., Ault, T. R., & Smerdon, J. E. (2015). Unprecedented 21st century drought risk in the American southwest and Central Plains. *Science Advances*, *1*(1), e1400082. https://doi.org/10.1126/sciadv.1400082
Cook, E. R., Seager, R., Heim, R. R., Vose, R. S., Herweijer, C., & Woodhouse, C. (2010). Megadroughts in North America: Placing IPCC projections of hydroclimatic change in a long-term palaeoclimate context. *Journal of Quaternary Science*, *25*(1), 48–61. https://doi.org/10.1002/jqs.1303
Coplen, T. B. (2007). Calibration of the calcite-water oxygen-isotope geothermometer at devils hole, Nevada, a natural laboratory. *Geochimica et Cosmochimica Acta*, *71*(16), 3948–3957. https://doi.org/10.1016/j.gca.2007.05.028
Cronin, T. M., Gemery, L., Briggs, W. M. Jr., Jakobsson, M., Polyak, L., & Brouwers, E. M. (2010). Quaternary Sea-ice history in the Arctic Ocean based on a new Ostracode Sea-ice proxy. *Quaternary Science Reviews*, *29*(25–26), 3415–3429. https://doi.org/10.1016/j.quascirev.2010.05.024
Cvijanovic, I., Santer, B. D., Bonfils, C., Lucas, D. D., Chiang, J. C. H., & Zimmerman, S. (2017). Future loss of Arctic Sea-ice cover could drive a substantial decrease in California's rainfall. *Nature Communications*, *8*(1), 1947. https://doi.org/10.1038/s41467-017-01907-4
Daëron, M., Drysdale, R. N., Peral, M., Huyghe, D., Blamart, D., Coplen, T. B., et al. (2019). Most earth-surface calcites precipitate out of isotopic equilibrium. *Nature Communications*, *10*(1), 429. https://doi.org/10.1038/s41467-019-08336-5
Davis, O. K. (1999). Pollen analysis of a late-glacial and Holocene sediment core from mono Lake, Mono County, California. *Quaternary Research*, *52*(2), 243–249. https://doi.org/10.1006/qres.1999.2063
De Vernal, A., Hillaire-Marcel, C., & Darby, D. A. (2005). Variability of sea ice cover in the Chukchi Sea (western Arctic Ocean) during the Holocene. *Paleoceanography*, *20*, PA4018. https://doi.org/10.1029/2005PA001157
Dettinger, M. D. (2013). Atmospheric Rivers as drought busters on the U.S. west coast. *Journal of Hydrometeorology*, *14*(6), 1721–1732. https://doi.org/10.1175/JHM-D-13-02.1
Diffenbaugh, N. S., Ashfaq, M., Shuman, B., Williams, J. W., & Bartlein, P. J. (2006). Summer aridity in the United States: Response to mid-Holocene changes in insolation and sea surface temperature. *Geophysical Research Letters*, *33*, L22712. https://doi.org/10.1029/2006GL028012
Dyke, A. S., Hooper, J., & Savelle, J. M. (1996). A history of sea ice in the Canadian Arctic archipelago based on postglacial remains of the bowhead whale (Balaena mysticetus). *Arctic*, *49*(3), 235–255. https://doi.org/10.14430/arctic1200
England, J. H., Lakeman, T. R., Lemmen, D. S., Bednarski, J. M., Stewart, T. G., & Evans, D. J. A. (2008). A millennial-scale record of Arctic Ocean sea ice variability and the demise of the Ellesmere Island ice shelves. *Geophysical Research Letters*, *35*, L19502. https://doi.org/10.1029/2008GL034470
Fairchild, I. J., & Baker, A. (2012). *Speleothem science: From process to past environments*. Oxford: Wiley-Blackwell.
Feng, X. H., & Epstein, S. (1994). Climatic implications of an 8000-year hydrogen isotope time-series from bristlecone-pine trees. *Science*, *265*(5175), 1079–1081. https://doi.org/10.1126/science.265.5175.1079
Fisher, D. A., Koerner, R. M., & Reeh, N. (1995). Holocene climatic records from Agassiz ice cap, Ellesmere Island, Nwt, Canada. *Holocene*, *5*(1), 19–24. https://doi.org/10.1177/095968369500500103
Fleck, J. (2016). *Water is for fighting over, and other myths about water in the West*. Washington, DC: Island Press.
Francis, J. A., Chan, W., Leathers, D. J., Miller, J. R., & Veron, D. E. (2009). Winter Northern Hemisphere weather patterns remember summer Arctic sea-ice extent. *Geophysical Research Letters*, *36*, L07503. https://doi.org/10.1029/2009GL037274
Friedman, I. (2002). Stable isotope compositions of waters in the Great Basin, United States 2. Modern precipitation. *Journal of Geophysical Research*, *107*(D19), 4401 https://doi.org/10.1029/2001JD000566
Funder, S., Goosse, H., Jepsen, H., Kaas, E., Kjær, K. H., Korsgaard, N. J., et al. (2011). A 10,000-year record of Arctic Ocean sea-ice variability—View from the beach. *Science*, *333*(6043), 747–750. https://doi.org/10.1126/science.1202760
Fyfe, J. C., Derksen, C., Mudryk, L., Flato, G. M., Santer, B. D., Swart, N. C., et al. (2017). Large near-term projected snowpack loss over the western United States. *Nature Communications*, *8*. https://doi.org/10.1038/ncomms14996
Garfin, G., Jardine, A., Merideth, R., Black, M., & LeRoy, S. (2013). *Assessment of climate change in the Southwest United States: A report prepared for the National Climate Assessment*. Washington, DC: Island Press.
Gershunov, A., Shulgina, T., Ralph, F. M., Lavers, D. A., & Rutz, J. J. (2017). Assessing the climate-scale variability of atmospheric rivers affecting western North America. *Geophysical Research Letters*, *44*, 7900–7908. https://doi.org/10.1002/2017GL074175
Graham, N. E., Hughes, M. K., Ammann, C. M., Cobb, K. M., Hoerling, M. P., Kennett, D. J., et al. (2007). Tropical Pacific-mid-latitude teleconnections in medieval times. *Climatic Change*, *83*(1-2), 241–285. https://doi.org/10.1007/s10584-007-9239-2
Grayson, D. K. (2000). Mammalian responses to middle Holocene climatic change in the Great Basin of the Western United States. *Journal of Biogeography*, *27*(1), 181–192. https://doi.org/10.1046/j.1365-2699.2000.00383.x
Grayson, D. K. (2011). *The Great Basin: A natural prehistory*. Berkeley, CA: University of California Press.
Hallett, D. J., & Anderson, R. S. (2010). Paleofire reconstruction for high-elevation forests in the Sierra Nevada, California, with implications for wildfire synchrony and climate variability in the late Holocene. *Quaternary Research*, *73*(2), 180–190. https://doi.org/10.1016/j.yqres.2009.11.008
Hanslik, D., Jakobsson, M., Backman, J., Björck, S., Sellén, E., O'Regan, M., et al. (2010). Quaternary Arctic Ocean sea ice variations and radiocarbon reservoir age corrections. *Quartenart Science Reviews*, *29*(25–26), 3430–3441. https://doi.org/10.1016/j.quascirev.2010.06.011
Harrison, S. P., Bartlein, P. J., & Prentice, I. C. (2016). What have we learnt from palaeoclimate simulations? *Journal of Quaternary Science*, *31*(4), 363–385. https://doi.org/10.1002/jqs.2842
Harrison, S. P., Kutzbach, J. E., Liu, Z., Bartlein, P. J., Otto-Bliesner, B., Muhs, D., et al. (2003). Mid-Holocene climates of the Americas: A dynamical response to changed seasonality. *Climate Dynamics*, *20*(7), 663–688. https://doi.org/10.1007/s00382-002-0300-6
Hereford, R., Webb, R. H., & Longpre, C. I. (2006). Precipitation history and ecosystem response to multidecadal precipitation variability in the Mojave Desert region, 1893-2001. *Journal of Arid Environments*, *67*(SUPPL), 13–34. https://doi.org/10.1016/j.jaridenv.2006.09.019

Hermann, N. W., Oster, J. L., & Ibarra, D. E. (2018). Spatial patterns and driving mechanisms of mid-Holocene hydroclimate in western North America. *Journal of Quaternary Science*, *33*(4), 421–434. https://doi.org/10.1002/jqs.3023

Huckleberry, G., Beck, C., Jones, G. T., Holmes, A., Cannon, M., Livingston, S., & Broughton, J. M. (2001). Terminal Pleistocene/early Holocene environmental change at the sunshine locality, north-Central Nevada, USA. *Quaternary Research*, *55*(3), 303–312. https://doi.org/10.1006/qres.2001.2217

Jana, S., Rajagopalan, B., Alexander, M. A., & Ray, A. J. (2018). Understanding the dominant sources and tracks of moisture for summer rainfall in the Southwest United States. *Journal of Geophysical Research: Atmospheres*, *123*, 4850–4870. https://doi.org/10.1029/2017JD027652

Kaufman, D. S., Ager, T. A., Anderson, N. J., Anderson, P. M., Andrews, J. T., & Bartlein, P. J. (2004). Holocene thermal maximum in the western Arctic (0–180°W). *Quaternary Science Reviews*, *23*(5-6), 529–560. https://doi.org/10.1016/j.quascirev.2003.09.007

Kay, J. E., Deser, C., Phillips, A., Mai, A., Hannay, C., Strand, G., et al. (2014). The community earth system model (CESM) large ensemble project: A community resource for studying climate change in the presence of internal climate variability. *Bulletin of the American Meteorological Society*, *96*(8), 1333–1349. https://doi.org/10.1175/BAMS-D-13-00255.1

Kirby, M. E., Feakins, S. J., Bonuso, N., Fantozzi, J. M., & Hiner, C. A. (2013). Latest Pleistocene to Holocene hydroclimates from Lake Elsinore, California. *Quaternary Science Reviews*, *76*, 1–15. https://doi.org/10.1016/j.quascirev.2013.05.023

Kirby, M. E., Knell, E. J., Anderson, W. T., Lachniet, M. S., Palermo, J., Eeg, H., et al. (2015). Evidence for insolation and Pacific forcing of late glacial through Holocene climate in the Central Mojave Desert (silver Lake, CA). *Quaternary Research*, *84*(2), 174–186. https://doi.org/10.1016/j.yqres.2015.07.003

Kirtman, B., Power, S. B., Adedoyin, J. A., Boer, G. J., Bojariu, R., & Camilloni, I. (2013). Near-term Climate Change: Projections and Predictability. In Stocker, T. F., Qin, D., Plattner, G.-K., Tignor, M., Allen, S. K., Boschung, J., Nauels, A., Xia, Y., Bex, V., & Midgley, P. M. (Eds.), *Climate Change 2013: The Physical Science Basis. Contribution of Working Group I to the Fifth Assessment Report of the Intergovernmental Panel on Climate Change*, (pp. 953–1028). Cambridge, United Kingdom and New York, NY, USA: Cambridge University Press.

Koutavas, A., & Joanides, S. (2012). El Niño–southern oscillation Extrema in the Holocene and last glacial maximum. *Paleoceanography*, *27*, PA4208. https://doi.org/10.1029/2012PA002378

Lachniet, M. S. (2016). Great Basin Paleoclimate from the leviathan chronology, Nevada. In C. G. Oviatt & J. F. Shroder (Eds.), *Lake Bonneville: A scientific update* (pp. 551–569). Amsterdam, The Netherlands: Elsevier.

Lachniet, M. S., Asmerom, Y., Polyak, V. P., & Denniston, R. F. (2017). Arctic cryosphere and Milankovitch forcing of Great Basin paleoclimate. *Scientific Reports*, *7*, 1–10. https://doi.org/10.1038/s41598-017-13279-2

Lachniet, M. S., Denniston, R. F., Asmerom, Y., & Polyak, V. J. (2014). Orbital control of western North America atmospheric circulation and climate over two glacial cycles. *Nature Communications*, *5*(1), 3805. https://doi.org/10.1038/ncomms4805

LaMarche, V. C. Jr. (1973). Holocene climatic variations inferred from treeline fluctuations in the White Mountains, California. *Quaternary Research*, *3*(4), 632–660. https://doi.org/10.1016/0033-5894(73)90035-5

Lindström, S. (1990). Submerged tree stumps as indicators of mid-Holocene aridity in the Lake Tahoe Basin. *Journal of California and Great Basin Anthropology*, *12*(2), 146–157. https://www.jstor.org/stable/27825419

Linsley, B. K., Rosenthal, Y., & Oppo, D. W. (2010). Holocene evolution of the Indonesian throughflow and the western Pacific warm pool. *Nature Geoscience*, *3*(578). https://doi.org/10.1038/ngeo920

Liu, Z., Brady, E., & Lynch-Stieglitz, J. (2003). Global Ocean response to orbital forcing in the Holocene. *Paleoceanography*, *18*(2), 1041. https://doi.org/10.1029/2002PA000819

Louderback, L. A., & Rhode, D. E. (2009). 15,000 years of vegetation change in the Bonneville basin: The blue Lake pollen record. *Quaternary Science Reviews*, *28*(3-4), 308–326. https://doi.org/10.1016/j.quascirev.2008.09.027

MacDonald, G. M., Moser, K. A., Bloom, A. M., Potito, A. P., Porinchu, D. F., Holmquist, J. R., et al. (2016). Prolonged California aridity linked to climate warming and Pacific Sea surface temperature. *Scientific Reports*, *6*, 33325. https://doi.org/10.1038/srep33325

Madsen, D. B. (2000). *Late Quaternary Paleoecology in the Bonneville Basin* (Vol. 130). Salt Lake City, UT: Utah Geological Survey Bulletin.

Madsen, D. B., & Currey, D. R. (1979). Late Quaternary glacial and vegetation changes, little cottonwood canyon area, Wasatch Mountains, Utah. *Quaternary Research*, *12*(2), 254–270. https://doi.org/10.1016/0033-5894(79)90061-9

Marsicek, J., Shuman, B. N., Bartlein, P. J., Shafer, S. L., & Brewer, S. (2018). Reconciling divergent trends and millennial variations in Holocene temperatures. *Nature*, *554*, 92. https://doi.org/10.1038/nature25464

McCabe-Glynn, S., Johnson, K. R., Strong, C., Zou, Y., Yu, J.-Y., Sellars, S., & Welker, J. M. (2016). Isotopic signature of extreme precipitation events in the western U.S. and associated phases of Arctic and tropical climate modes. *Journal of Geophysical Research: Atmospheres*, *121*, 8913–8924. https://doi.org/10.1002/2016JD025524

Meehl, G. A., & Hu, A. (2006). Megadroughts in the Indian monsoon region and Southwest North America and a mechanism for associated multidecadal Pacific Sea surface temperature anomalies. *Journal of Climate*, *19*(9), 1605–1623. https://doi.org/10.1175/JCLI3675.1

Meko, D. M., Woodhouse, C. A., Baisan, C. A., Knight, T., Lukas, J. J., Hughes, M. K., & Salzer, M. W. (2007). Medieval drought in the upper Colorado River Basin. *Geophysical Research Letters*, *34*, L10705. https://doi.org/10.1029/2007GL029988

Mensing, S. A., Benson, L. V., Kashgarian, M., & Lund, S. (2004). A Holocene pollen record of persistent droughts from Pyramid Lake, Nevada, USA. *Quaternary Research*, *62*(1), 29–38. https://doi.org/10.1016/j.yqres.2004.04.002

Mensing, S. A., Sharpe, S. E., Tunno, I., Sada, D. W., Thomas, J. M., Starratt, S., & Smith, J. (2013). The Late Holocene dry period: Multiproxy evidence for an extended drought between 2800 and 1850 cal yr BP across the central Great Basin, USA. *Quaternary Science Reviews*, *78*, 266–282. https://doi.org/10.1016/j.quascirev.2013.08.010

Metcalfe, S. E., Barron, J. A., & Davies, S. J. (2015). The Holocene history of the north American monsoon: 'Known knowns' and 'known unknowns' in understanding its spatial and temporal complexity. *Quaternary Science Reviews*, *120*, 1–27. https://doi.org/10.1016/j.quascirev.2015.04.004

Millar, C. I., Charlet, D. A., Delany, D. L., King, J. C., & Westfall, R. D. (2018). Shifts of demography and growth in limber pine forests of the Great Basin, USA, across 4000 yr of climate variability. *Quaternary Research*, *91*(2), 691–704. https://doi.org/10.1017/qua.2018.120

Mote, P. W., Li, S., Lettenmaier, D. P., Xiao, M., & Engel, R. (2018). Dramatic declines in snowpack in the western US. *npj. Climate and Atmospheric Science*, *1*(1). https://doi.org/10.1038/s41612-018-0012-1

Müller, J., Werner, K., Stein, R., Fahl, K., Moros, M., & Jansen, E. (2012). Holocene cooling culminates in sea ice oscillations in Fram Strait. *Quaternary Science Reviews*, *47*, 1–14. https://doi.org/10.1016/j.quascirev.2012.04.024

Oglesby, R., Feng, S., Hu, Q., & Rowe, C. (2012). The role of the Atlantic multidecadal oscillation on medieval drought in North America: Synthesizing results from proxy data and climate models. *Global and Planetary Change*, *84-85*, 56–65. https://doi.org/10.1016/j.gloplacha.2011.07.005

Oster, J. L., Sharp, W. D., Covey, A. K., Gibson, J., Rogers, B., & Mix, H. (2017). Climate response to the 8.2 ka event in coastal California. *Scientific Reports*, *7*(1), 3886. https://doi.org/10.1038/s41598-017-04215-5

Overland, J. E., Dethloff, K., Francis, J. A., Hall, R. J., Hanna, E., Kim, S.-J., et al. (2016). Nonlinear response of mid-latitude weather to the changing Arctic. *Nature Climate Change*, *6*(11), 992–999. https://doi.org/10.1038/nclimate3121

Park, H.-S., Kim, S.-J., Stewart, A. L., Son, S.-W., & Seo, K.-H. (2019). Mid-Holocene northern hemisphere warming driven by Arctic amplification. *Science Advances*, *5*(12), eaax8203. https://doi.org/10.1126/sciadv.aax8203

Polyak, V. J., & Asmerom, Y. (2001). Late Holocene climate and cultural changes in the southwestern United States. *Science*, *294*(5540), 148–151. https://doi.org/10.1126/science.1062771

Polyakov, I. V., Alexeev, V. A., Bhatt, U. S., Polyakova, E. I., & Zhang, X. (2010). North Atlantic warming: Patterns of long-term trend and multidecadal variability. *Climate Dynamics*, *34*(2), 439–457. https://doi.org/10.1007/s00382-008-0522-3

Quade, J. (1986). Late Quaternary environmental changes in the upper Las Vegas Valley, Nevada. *Quaternary Research (New York)*, *26*(3), 340–357. https://doi.org/10.1016/0033-5894(86)90094-3

Quade, J., Cerling, T. E., & Bowman, J. R. (1989). Systematic variations in the carbon and oxygen isotopic composition of pedogenic carbonate along elevation transects in the southern Great Basin, United States; with Suppl. Data 89-10. *Geological Society of America Bulletin*, *101*(4), 464–475. https://doi.org/10.1130/0016-7606(1989)101<0464:SVITCA>2.3.CO;2

Quade, J., Forester, R. M., Pratt, W. L., & Carter, C. (1998). Black mats, spring-fed streams, and late-glacial-age recharge in southern Great Basin. *Quaternary Research (New York)*, *49*(2), 129–148. https://doi.org/10.1006/qres.1997.1959

Renssen, H., Goosse, H., Fichefet, T., Brovkin, V., Driesschaert, E., & Wolk, F. (2005). Simulating the Holocene climate evolution at northern high latitudes using a coupled atmosphere-sea ice-ocean-vegetation model. *Climate Dynamics*, *24*(1), 23–43. https://doi.org/10.1007/s00382-004-0485-y

Renssen, H., Seppä, H., Crosta, X., Goosse, H., & Roche, D. M. (2012). Global characterization of the Holocene thermal maximum. *Quaternary Science Reviews*, *48*, 7–19. https://doi.org/10.1016/j.quascirev.2012.05.022

Routson, C. C., McKay, N. P., Kaufman, D. S., Erb, M. P., Goosse, H., Shuman, B. N., et al. (2019). Mid-latitude net precipitation decreased with Arctic warming during the Holocene. *Nature*, *568*(7750), 83–87. https://doi.org/10.1038/s41586-019-1060-3

Routson, C. C., Woodhouse, C. A., & Overpeck, J. T. (2011). Second century megadrought in the Rio Grande headwaters, Colorado: How unusual was medieval drought? *Geophysical Research Letters*, *38*, L22703. https://doi.org/10.1029/2011GL050015

Rozanski, K., Araguás-Araguás, L., & Gonfiantini, R. (1993). Isotopic patterns in modern global precipitation. In Swart, P. K., Lohmann, K. L., McKenzie, J., & Savin, S. (Eds.), *Climate Change in Continental Isotopic Records*, *Geophysical monograph*, (1–37 ed., Vol. 78, pp. 1–37). Washington, DC: American Geophysical Union.

Salathé, E. P. (2006). Influences of a shift in North Pacific storm tracks on western North American precipitation under global warming. *Geophysical Research Letters*, *33*, L19820. https://doi.org/10.1029/2006GL026882

Salzer, M. W., Bunn, A. G., Graham, N. E., & Hughes, M. K. (2014). Five millennia of paleotemperature from tree-rings in the Great Basin USA. *Climate Dynamics*, *42*(5–6), 1517–1526. https://doi.org/10.1007/s00382-013-1911-9

Schmidt, G. A., Annan, J. D., Bartlein, P. J., Cook, B. I., Guilyardi, E., Hargreaves, J. C., et al. (2014). Using palaeo-climate comparisons to constrain future projections in CMIP5. *Climate of the Past*, *10*(1), 221–250. https://doi.org/10.5194/cp-10-221-2014

Scuderi, L. A. (1987). Late-Holocene upper timberline variation in the southern sierra-Nevada. *Nature*, *325*(6101), 242–244. https://doi.org/10.1038/325242a0

Seager, R., Hoerling, M., Schubert, S., Wang, H., Lyon, B., Kumar, A., et al. (2015). Causes of the 2011–14 California drought. *Journal of Climate*, *28*(18), 6997–7024. https://doi.org/10.1175/JCLI-D-14-00860.1

Seager, R., & Vecchi, G. A. (2010). Greenhouse warming and the 21st century hydroclimate of southwestern North America. *Proceedings of the National Academy of Sciences*, *107*(50), 21,277–21,282. https://doi.org/10.1073/pnas.0910856107

Serreze, M. C., Clark, M. P., Armstrong, R. L., McGinnis, D. A., & Pulwarty, R. S. (1999). Characteristics of the western United States snowpack from snowpack telemetry (SNOTEL) data. *Water Resources Research*, *35*(7), 2145–2160. https://doi.org/10.1029/1999WR900090

Sewall, J. O. (2005). Precipitation shifts over Western North America as a result of declining Arctic Sea ice cover: The coupled system response. *Earth Interactions*, *9*(1), 1–23. https://doi.org/10.1175/ei171.1

Shakun, J. D., Burns, S. J., Clark, P. U., Cheng, H., & Edwards, R. L. (2011). Milankovitch-paced Termination II in a Nevada speleothem. *Geophysical Research Letters*, *38*, L18701. https://doi.org/10.1029/2011GL048560

Sheridan, S. C. (2002). The redevelopment of a weather-type classification scheme for North America. *International Journal of Climatology*, *22*(1), 51–68. https://doi.org/10.1002/joc.709

Shuman, B., Pribyl, P., Minckley, T. A., & Shinker, J. J. (2010). Rapid hydrologic shifts and prolonged droughts in Rocky Mountain headwaters during the Holocene. *Geophysical Research Letters*, *37*, L06701. https://doi.org/10.1029/2009GL042196

Shuman, B. N., & Serravezza, M. (2017). Patterns of hydroclimatic change in the Rocky Mountains and surrounding regions since the last glacial maximum. *Quaternary Science Reviews*, *173*, 58–77. https://doi.org/10.1016/j.quascirev.2017.08.012

Spaulding, W. G. (1991). A middle Holocene vegetation record from the Mojave Desert of North-America and its Paleoclimatic significance. *Quaternary Research*, *35*(3), 427–437. https://doi.org/10.1016/0033-5894(91)90055-a

Steponaitis, E., Andrews, A., McGee, D., Quade, J., Hsieh, Y.-T., Broecker, W. S., et al. (2015). Mid-Holocene drying of the U.S. Great Basin recorded in Nevada speleothems. *Quaternary Science Reviews*, *127*, 174–185. https://doi.org/10.1016/j.quascirev.2015.04.011

Stott, L., Cannariato, K., Thunell, R., Haug, G. H., Koutavas, A., & Lund, S. (2004). Decline of surface temperature and salinity in the western tropical Pacific Ocean in the Holocene epoch. *Nature*, *431*(7004), 56–59. https://doi.org/10.1038/nature02903

Stranne, C., Jakobsson, M., & Björk, G. (2014). Arctic Ocean perennial sea ice breakdown during the Early Holocene insolation maximum. *Quaternary Science Reviews*, *92*, 123–132. https://doi.org/10.1016/j.quascirev.2013.10.022

Swain, D. L., Singh, D., Horton, D. E., Mankin, J. S., Ballard, T. C., & Diffenbaugh, N. S. (2017). Remote linkages to anomalous winter atmospheric ridging over the northeastern Pacific. *Journal of Geophysical Research: Atmospheres*, *122*, 12,194–12,209. https://doi.org/10.1002/2017JD026575

Thompson, R. S. (1992). Late Quaternary environments in Ruby Valley, Nevada. *Quaternary Research*, *37*(1), 1–15. https://doi.org/10.1016/0033-5894(92)90002-z

Thompson, R. S., Whitlock, C., Bartlein, P. J., Harrison, S. P., & Spaulding, W. G. (1993). Climatic changes in the Western United States since 18,000 yr BP. In J. H. E. Wright (Ed.), *Global climates since the Last Glacial Maximum* (pp. 468–513). Minneapolis: University of Minnesota Press.

Udall, B., & Overpeck, J. (2017). The twenty-first century Colorado River hot drought and implications for the future. *Water Resources Research*, *53*, 2404–2418. https://doi.org/10.1002/2016WR019638

Vare, L. L., Massé, G., Gregory, T. R., Smart, C. W., & Belt, S. T. (2009). Sea ice variations in the central. *Canadian Arctic Archipelago during the Holocene*, *28*(13–14), 1354–1366. https://doi.org/10.1016/j.quascirev.2009.01.013

Waelbroeck, C., Labeyrie, L., Michel, E., Duplessy, J. C., McManus, J. F., Lambeck, K., et al. (2002). Sea-level and deep water temperature changes derived from benthic foraminifera isotopic records. *Quaternary Science Reviews*, *21*(1–3), 295–305. https://doi.org/10.1016/s0277-3791(01)00101-9

Wang, S.-Y., Hipps, L., Gillies, R. R., & Yoon, J.-H. (2014). Probable causes of the abnormal ridge accompanying the 2013–2014 California drought: ENSO precursor and anthropogenic warming footprint. *Geophysical Research Letters*, *41*(9), 3220–3226. https://doi.org/10.1002/2014gl059748

Webb, R. H., & Betancourt, J. L. (1990). The spatial and temporal distribution of radiocarbon ages from packrat middens. In Betancourt, J. L., van Devender, T. R., & Martin, P. S. (Eds.), *Packrat Middens: The Last 40,000 Years of Biotic Change*, (pp. 85–102). Tucson: Univ. of Arizona Press.

Wigand, P. E. (1987). Diamond pond, Harney County, Oregon: Vegetation history and water table in the eastern Oregon desert. *Great Basin Naturalist*, *47*, 427–458.

Wigand, P. E., & Rhode, D. (2002). Great Basin vegetation history and aquatic systems: The last 150,000 years. In *Great Basin Aquatic Systems History*, (pp. 309–367). Washington, D.C.: Smithsonian.

Williams, A. P., Cook, E. R., Smerdon, J. E., Cook, B. I., Abatzoglou, J. T., Bolles, K., et al. (2020). Large contribution from anthropogenic warming to an emerging north American megadrought. *Science*, *368*(6488), 314–318. https://doi.org/10.1126/science.aaz9600

Winograd, I. J., Riggs, A. C., & Coplen, T. B. (1998). The relative contributions of summer and cool-season precipitation to groundwater recharge, Spring Mountains, Nevada, USA. *Hydrogeology Journal*, *6*(1), 77–93. https://doi.org/10.1007/s100400050135

Wong, C. I., & Breecker, D. O. (2015). Advancements in the use of speleothems as climate archives. *Quaternary Science Reviews*, *127*, 1–18. https://doi.org/10.1016/j.quascirev.2015.07.019

Woodhouse, C. A., Meko, D. M., MacDonald, G. M., Stahle, D. W., & Cook, E. R. (2010). A 1,200-year perspective of 21st century drought in southwestern North America. *Proceedings of the National Academy of Sciences*, *107*(50), 21283. https://doi.org/10.1073/pnas.0911197107

Woodhouse, C. A., Pederson, G. T., Morino, K., McAfee, S. A., & McCabe, G. J. (2016). Increasing influence of air temperature on upper Colorado River streamflow. *Geophysical Research Letters*, *43*, 2174–2181. https://doi.org/10.1002/2015GL067613

Yoshimori, M., & Suzuki, M. (2019). The relevance of mid-Holocene Arctic warming to the future. *Climate of the Past*, *15*(4), 1375–1394. https://doi.org/10.5194/cp-15-1375-2019

Zhang, Q., Sundqvist, H. S., Moberg, A., Kornich, H., Nilsson, J., & Holmgren, K. (2010). Climate change between the mid and late Holocene in northern high latitudes - part 2: Model-data comparisons. *Climate of the Past*, *6*(5), 609–626. https://doi.org/10.5194/cp-6-609-2010

Ziegler, M., Nürnberg, D., Karas, C., Tiedemann, R., & Lourens, L. J. (2008). Persistent summer expansion of the Atlantic warm Pool during glacial abrupt cold events. *Nature Geoscience*, *1*(9), 601–605. https://doi.org/10.1038/ngeo277